Features of Auditory Brainstem Response Spectral Representations as Tools for ADHD-Diagnostics

Edwin Klint Bywater

September 15, 2014

Abstract

ADHD is a psychological disorder which has become significantly more prevalent and much debated in the last decades. This study investigates the possibilities in developing quantitative diagnostic tools for psychiatric assessment of ADHD based on spectral representations of Auditory Brainstem Responses (ABR). Two different approaches to data pre-treatment are adopted, followed by estimates of power spectral densities, cross power spectral densities and time-frequency distributions. From these, features are extracted and examined on their merit as disorder-specific traits. The subject sample consists of ABR:s from 69 individuals; 36 of which are diagnosed with ADHD and 33 healthy controls. Using a band-pass pre-processing method, some significance in difference between disease groups is found for females in terms of dominant frequency*, bandwidth****, spectral purity*** and spectral slope* in the power spectral density estimate.

Keywords

Bioinformatics, Auditory Brainstem Response, ADHD, Quantitative Psychology, Signal Processing, Spectral Analysis, Time-Frequency Analysis, Hjorth Descriptors, Entropy

Acknowledgements

I wish to thank my supervisor Maria Sandsten for her perceptive guidance and expertise, and for the flexible and stimulating work environment that followed. Her enthusiasm for my ideas and progress has been a true inspiration as this thesis took shape.

I would also like to thank the staff at SensoDetect AB, whose acquaintance and further co-operation has been a pleasure and has equipped me with valuable experience in research. In particular, I would like to mention Johan Källstrand for providing me with data as well as an insightful dialogue on numerous occasions, and Jens Holmberg for his vital input and curiosity surrounding my thesis and related research.

Edwin Klint Bywater, Lund, May 2014

List of Notations

Glossary

ABR - Auditory Brainstem Response.

ADHD - Attention Deficient Hyperactive Disorder.

CPSD - Cross power spectral density.

EEG - Electroencephalography.

ERP - Event related potentials.

PSD - Power spectral density.

TFD - Time-frequency distribution.

Mathematical quantities

f - Absolute frequency in Hz.

$S_x(f)$ - Power spectral density of a signal x_t.

t - The intra-observational time, in sampled data points.

T - The global time, in sampled data points.

u - The global time, in number of observations.

$W_z(n,k)$ - The discrete time-frequency distribution of an analytic signal z_t.

x_t - An ABR-observation (discrete time).

$x_{t,T}$ - A full set of ABR-observations with observations as column in a matrix with t rows and T column.

$\bar{x}_t$ - The mean over some number of observations.

z_t - Analytic signal, the Hilbert transform of a signal x_t.

$\Gamma_{x_1,x_2}(f)$ - Cross power spectral density of signals $x_{1,t},\ x_{2,t}$.

$\Theta_{M,\Lambda,\varphi,\xi,h}$ - Feature of type $\varphi = \{\mathcal{H}_1, \mathcal{H}_2, \mathcal{I}, \mathcal{K}, \mathcal{E}_1, \mathcal{E}_2, \mathcal{P}\}$ from $\Lambda = \{\text{PSD,CPSD,TFD}\}$ using data-treatment method $M = \{\text{win, b-p}\}$, test subject ξ and cerebral hemisphere $h = \{\text{L,R,B}\}$ (Left, Right, comparison between Both)

ξ - Test subject or group given by F for female, M for male, A for ADHD, C for healthy control, and a number within this set. e.g. $\xi = FA12$ for the 12th female in the ADHD-group, $\xi = M$ for all males or $\xi = C$ for all persons in the control group.

Contents

1 Introduction

1.1 Neuroscience and its Impact

It is safe to say that the scientific fields that in any way involve the human brain are at the forefront in today's technological landscape. The evolution, workings and possibilities of our very own cognitive apparatus poses thrilling questions that have been, and will be, around for centuries. Although it could be said that few other sciences have been as revolutionized by recent technological progress, much remains to be understood and gained by treating neuroscience as a branch of engineering.

The brain marks a starting point, not only for the way we all think and perceive the world, but for several branches of scientific inquiry. Related subjects extend from questions previously only regarded as philosophical, e.g. those of free will [1] and what constitutes spiritual experiences [2], to more practical issues such as understanding the connection between neurophysiology and emotional behaviour [3] or drawing inter-species comparisons [7]. In terms of applications, emerging fields are *neural prostheses*; replacements for impaired parts of the nervous system [4], and *neurorobotics*; controlling machinery [5] or prosthetic limbs [6] by thought alone.

The many branches of neuroscience involve medically complexity, engineering challenges and socio-societal ramification of vast proportion. Advances in brain research determine the way we understand cognition, something which is indispensable in an age where everyday computing more and more takes the shape of machine-human interaction[1], and they help us understand ourselves in terms of conscious tasks [9] and spontaneous, innate behaviours [10] alike. As diverse topics as political attitudes [11], [12] and food preferences [13] are now studied with the aid of *neural correlates*; linking brain with behaviour using *neuroimaging* techniques, there have even been stunning examples of court case verdicts reliant on such technology [14]. Lastly and perhaps most importantly, many questions concerning *mental illnesses and conditions* that affect millions worldwide remain unanswered. With today's progress in data analysis in mind, the domain of *psychiatric diagnostics* faces radical new possibilities in screening for and understanding such illnesses using *quantitative methods*, the topic to which this master's thesis attempts to contribute.

[1] ERP, Event Related Potentials, is the technique considered in this study. ERP is not rarely used as, or in assesment of, brain-compter interfaces [8].

1.2 ADHD in Psychiatry and Society

The treatment of data in the present study is aimed at finding *traits* for ADHD (Attention Deficit Hyperactivity Disorder), a disorder impairing a persons ability to give everyday tasks undivided attention. Short-term memory as well as impulse control is affected, in some sub-types of ADHD other symptoms that might arise are aggression [15] and excessive attachment [16]. ADHD in individuals is commonly discovered during childhood, making its assessment vulnerable to confusion; that between 'deficit' impulse control and normal childlike playfulness, curious nature and 'bouncyness'. This difficulty along with the fact that the prevalence of ADHD has risen significantly in the past decades [17], [18] has spurn a hot debate [19], [20], [21] around the validity of the diagnosis altogether, and certainly about the prescribed medication[2] as well as on the topic of child psychology as a whole.

Evidently, there is a great deal of motivation for studying this type of mental disorder, and put its current application into question. Naturally, settling the concerns around ADHD would be much helped by quantitative reasoning with a firm foundation in neurophysiology. It is certainly not beneficial for children, parents or the confidence put into the psychiatric community if an issue as widely disputed, and crucial for social- and learning conditions during childhood, as ADHD be subject to guessing and practices that are left unquestioned. This is not only true for ADHD, but for any field of neuroscience where we have only scratched the surface in terms of how quantitative methods may assist clinical judgement. To follow, in Sections 1.3 and 1.4, is some background on the brain's electrical properties and how these are measured using neuroimaging techniques. In Section 1.5, research questions and hypotheses are found, describing the possible link between such techniques and diagnostics and providing some justification for the *features* considered as potential ADHD-traits.

1.3 Electrophysiology of the Brain

All neural communication, and thus any cognitively planned and several unconscious physiological processes, is transmitted electrically in our bodies. In the brain, this feat of biological ingenuity is performed by means of ion channels containing, among others, sodium $\left(Na^{+}\right)$ and potassium $\left(K^{+}\right)$ ions. These ions fluctuate in and out of the cell membrane creating changes in electrical charge, which travels to neighbouring neurons along *axons* if certain voltage thresholds are exceeded. These travelling charges are called *action potentials*, the sum of which make up the electrical activity measured and considered in this study. A brief account of neural anatomy and these potentials is found in Figures 1 and 2.

[2] Most commonly Methylphenidate (Ritalin), controversial for its side effects [22], [23].

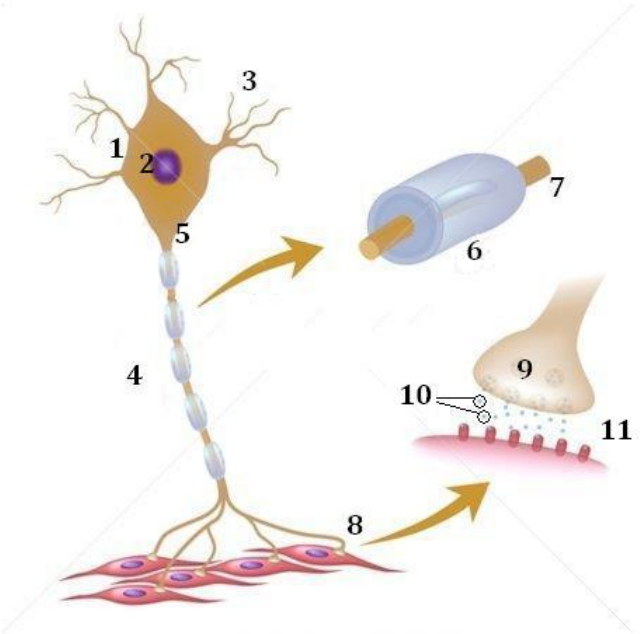

Figure 1: Depiction of a neuron with the cell body, *soma* (1) which like any bodily cell contains a *nucleus* (2). The *dendrites* (3) are responsible for recieving input from connected neurons. The output is in turn carried through the *axon* (4). This output are the *action potentials* that make up the vast majority of the electrical activity seen in the brain. The *axon hillock* (5) , where the soma extends to the axon, encompasses a voltage threshold (c.f. Figure 2), preventing 'false firings'. The action potential are generated and propagated by charge-carrying ions, mentioned above. For purposes of metabolic optimization, *myelin cells* (6) insulate the axons partially. These leave room, the so called *nodes of Ranvier* (7), between which ions may travel; a process known as saltatory conduction. The *axon terminal* (8) contains *synapses* (9) that, as an effect of the action potential, emit *neurotransmitter chemicals* (10). These carry instructions to the receiving neuron across the synaptic cleft (11). Neural resources: [33], [24]. Image source: [60].

An illustration of an action potential is seen in Figure 2. These potentials activate the receiving neuron, and 'cascades' of such activation and deactivation, along with the specific neurotransmitters emitted at the axon terminals, is what comprises neural communication.

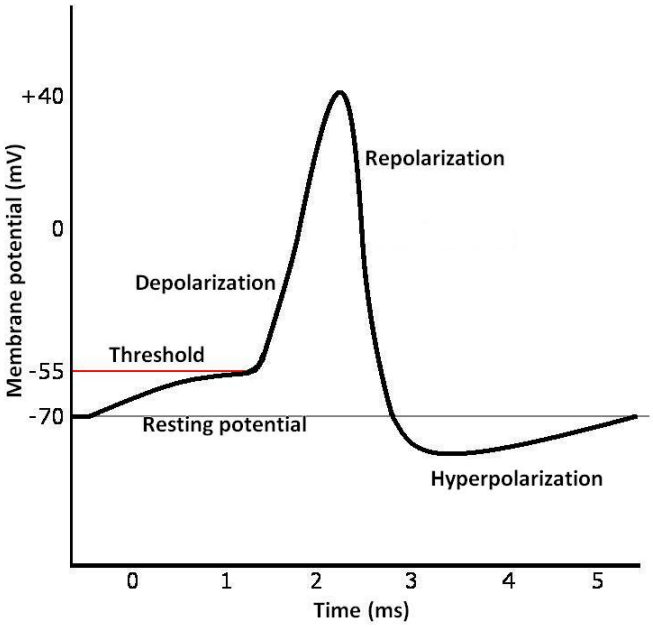

Figure 2: The mechanics of neuroelectircal transmission is highly binary; failing to exceed the *threshold* (~ -55 mV) at the axon hillock (c.f. Figure 1), yields no potential. Furthermore, action potentials from a given neuron are more or less constant in voltage. The action potential can be divided into three main phases. The first phase, *depolarization*, stems from a rapid change in membrane potential from *resting potential* (~ -70 mV) or just above it to, commonly, +40 mV. Here, certain voltage-gated ion channels in the cell membrane see increased permeability and thus an **influx** of $\left(\mathrm{Na}^{+}\right)$ ions. The second phase, *repolarization*, is a return towards the resting potential of the membrane and occurs when all sodium ions have been absorbed by the soma, after which $\left(\mathrm{K}^{+}\right)$ channels activate that let these potassium ions **out** through the membrane. The third phase, *hyperpolarization*, is a slight and slowly re-establishing undershoot of the resting potential, due to the potassium channels not closing entirely abruptly. The depolarization of the cell membrane generates currents that, in turn, depolarise adjacent parts of the axon membrane, and the action potential will propagate along down the axon so long as it exceeds local thresholds (that are typically lower that the one at the axon hillock.) Sources on action potentials [35] [33]. Image source: [61].

Single neuron action potentials of the brain are very rarely shorter than 1 ms, amounting to a lower limit for the region of interest in terms of wavelength, or an upper limit in terms of frequency. At a higher, *neuronal cluster* level, information is transmitted by propagation and intercommunicating between several neurons, and the collected activity recorded over large cerebral regions are typically much longer in duration[3]. However, the 'primitive' processes of the brainstem, and other 'old'[4] cerebral structures are faster, inherent of their relatively low complexity and neuronal density. For instance, as we shall see in Figure 3, the ABR typically comprises ~ 7 waves during 10 ms.

1.4 Neuroelectrical Imaging: EEG, ERP, ABR

EEG, electroencephalography, is the technique of measuring electrical properties of the brain using extra-cranial[5] electrodes. More specifically, when EEG is conducted so that the recorded neural activity is limited as to correspond to a specific, repeated stimulus[6], this is called Event Related Potentials (ERP). In ERP, it is assumed that the stimulus is distinct enough to give rise to more or less identical neural responses with each repetition. Hence, one may perform some form of averaging over these ERP-*observations* as a way to reduce noise and arrive at a *characteristic response*, the quantity we shall attempt to extract from data as described in Section 3.

Auditory Brainstem Response (ABR) refers to the particular kind of ERP where the aforementioned stimulus is sound, usually and in the case at hand, in the shape of distinct 'clicks' at given intervals, and where electrodes are placed and calibrated so as to study the processing that occurs in the basic auditory pathways, situated in the brainstem, Figure 3. That is to say, the later responses from cerebral clusters of higher processing complexity[7] are left out. Indeed, *Auditory Evoked Potentials* are sometimes studied up to half a second post-stimuli, capturing the later, cognitive auditory processing. As an example, this has been used to show differences in the brains of musicians and non-musicians [26]. In the following, only wanting brainstem activity, the available data extends to only 15 ms post stimuli. In this way, the obtained

[3]For instance terminology in EEG talks about 'alpha', 'beta', 'gamma' waves, and so forth. These are in the range of [Delta waves: $(0.1 - 3$ Hz$)$, Gamma waves: $(32 - 100$ Hz$)$] and primarily say something about various levels of wakefulness or physical and mental activity [55], [56]

[4]In terms of natural evolution. There is well-established evidence to suggest that our brain has not so much evolved as seen the addition of superstructures [25].

[5]Electrocorticography, (ECoG) is the name given to neural measurements from inside of the cranium, although this technique is far more accurate it is, for obvious reasons, more complex, expensive and uncomfortable for the test subject or patient.

[6]Rather than monitoring brain activity as a whole over a longer period of time, which is the primary usage of standard EEG.

[7]In particular the primary auditory cortex of the temporal lobe.

signals are less affected by a test subjects concious thoughts, memories or preferences attached to the induced sound. It is assumed throughout ABR-analysis that this exclusion of post-brainstem responses provides a clearer picture of the deeper cerebral functions more inherent to the individual subject.

At least since the 1960s, ABR has been applied to paediatrics [27]. Hereby, quality of hearing in infants can be determined, as it is a hard fought task to ask newborns about their auditory experiences. However, new areas of application have emerged in later years, among them the questions similar to the that posed by this study, namely within psychiatric diagnostics. Possibly, ABR could help to determine what illness or condition a patient has or is about to develop. For instance, there is strong evidence to suggest that ABR is reliable in diagnosing subjects with schizophrenia [28], a disease whose characteristics do include elements of auditory hallucinations [29], as well as Asperger syndrome [30].

From a physiological viewpoint, one is often interested in relating the peaks that can be seen in the ABR with actual regions in the brainstem. A timeline of an ABR, with the corresponding regions and pathways in the central auditory system, can be seen in Figure 3 below.

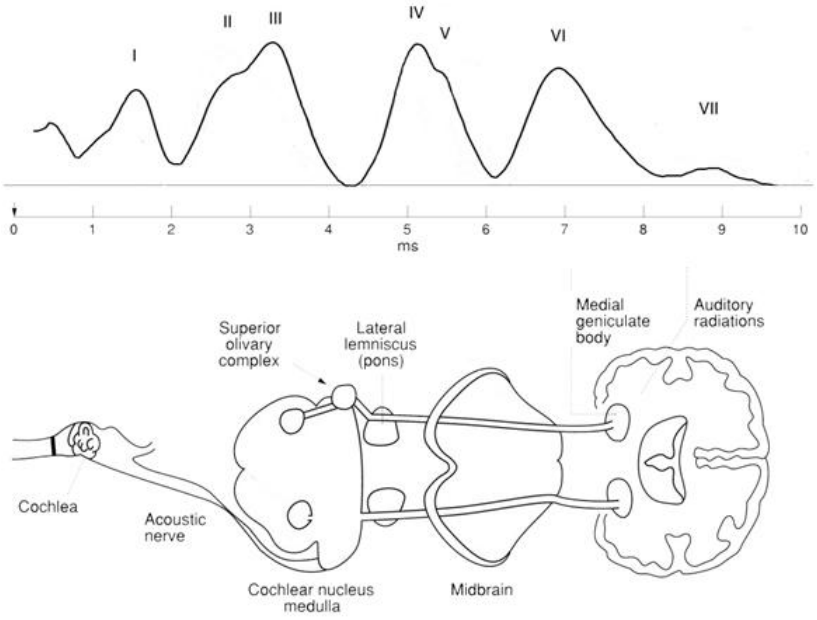

Figure 3: Timeline of an idealized ABR aligned with the regions in the brainstem auditory pathway from which waves labeled I-VII are understood to arise. Note that this only extends to 10 ms, whereafter responses from higher order cerebral structures are usually seen in the recording. The *cochlea* is part of the inner ear, containing the perilymph, a liquid set in motion by vibrations having passed through the early mechanical sound processing of the outer- and middle ear. In turn, the moving fluid affects hair cells that encode the vibrations into electrical communication. This is passed through the *acoustic, or vestibulocochlear, nerve* to the *cochlear nucleus*, whose primary function is preserving timing information of the incoming sound, for purposes such as source location. Further along is the *superior olivary complex*, acting as the primary site for auditory information from the left and right ears to start converging partially. The *lateral lemniscus* is a belt of axons of which relatively little is known, it does however transmit the auditory information maintaining good temporal resolution. The *inferior colliculus in the midbrain* has many purposes in auditory processing, among them pitch detection, amplitude modulation and further auditory pathway convergence. The *medial geniculate body*, part of the thalamus which acts as the brains major 'switchboard', relays the auditory information from the brainstem to the auditory cortex. Sources on auditory pathway: [31], [32], [33, ch.10], [34]. Image source: [59].

1.5 Outline and Hypotheses

Investigating time-dependent phenomena is the most common way to establish neurological traits from ABR for diagnostic purposes, and makes it possible to quantify *latency shifts* between test subjects or observations from a single test subject. In association with clinical research, it is then possible to make claims about delays in given peaks (I-VII), i.e. a delay from a given 'link' of the brainstem auditory pathway illustrated in Figure 3. Aside from latency, it is also possible to study the amplitude of one or more of the peaks in order to judge whether the physiological functionality of any corresponding link may be impaired, signified by distinctly larger or smaller local amplitude. This study, however, will adopt an approach of trait extraction from ABR:s, founded in *spectral analysis*. This is seen more rarely for ABR, or in other applications of ERP for that matter, but for instance in [41], [42]. In the following, we will work under the premise that examining frequency content in the ABR-data renders it possible to draw assumptions about the *synchronicity* of the brainstem neural communication, as well as the diversity of the spectral content, i.e. the variation in action potential duration among brainstem auditory pathway neurons. As an illustration, consider Figure 4 below.

Shown in Figure 4 are some coarse simulations made to demonstrate additions of simultaneous action potential firings. The various stages in the auditory pathway is made up by nothing other than action potentials firing more or less synchronized. As can be seen from Figures 4 a, b, c, difference in the delay between two action potentials gives rise to different wavelengths (frequencies) and for that matter number of wavelengths (bandwidth) present. We may thus draw the assumption that a lower dominant frequency in the ABR-response correlates with a less distinct response, and thus less synchronicity, and that a greater diversity in synchronicity is marked by greater bandwidth. By this reasoning, measures of dominant frequency and bandwidth are chosen as features. Specifically, the estimators of these two quantities used here are the so called *Hjorth descriptors* $\mathcal{H}_1$ and $\mathcal{H}_2$ respectively. For the reason mentioned above - ERP:s are rarely studied with the aid of spectral representations - Hjorth descriptors are uncommon in analysis of ERP, but have found wide usage within the EEG- [43] and ECG[8]-techniques [44]. Furthermore, we will look at the *spectral purity index*, $\mathcal{I}$, a measure of the degree to which a signal is described by a single sinusoid. We shall also consider the *spectral slope*, $\mathcal{K}$, which will tell us something about he ratio between low- and high frequency content within the signal. Further, we will make use of two kinds of *generalized Rényi entropies*, $\mathcal{E}_1$ and $\mathcal{E}_2$, and finally, we shall consider *power in frequency bands*, $\mathcal{P}$ (Section 2.2.1. This is a more adapted approach which is designed after spectral analysis.

[8]Electrocardiology, measuring the hearts electrical activity.

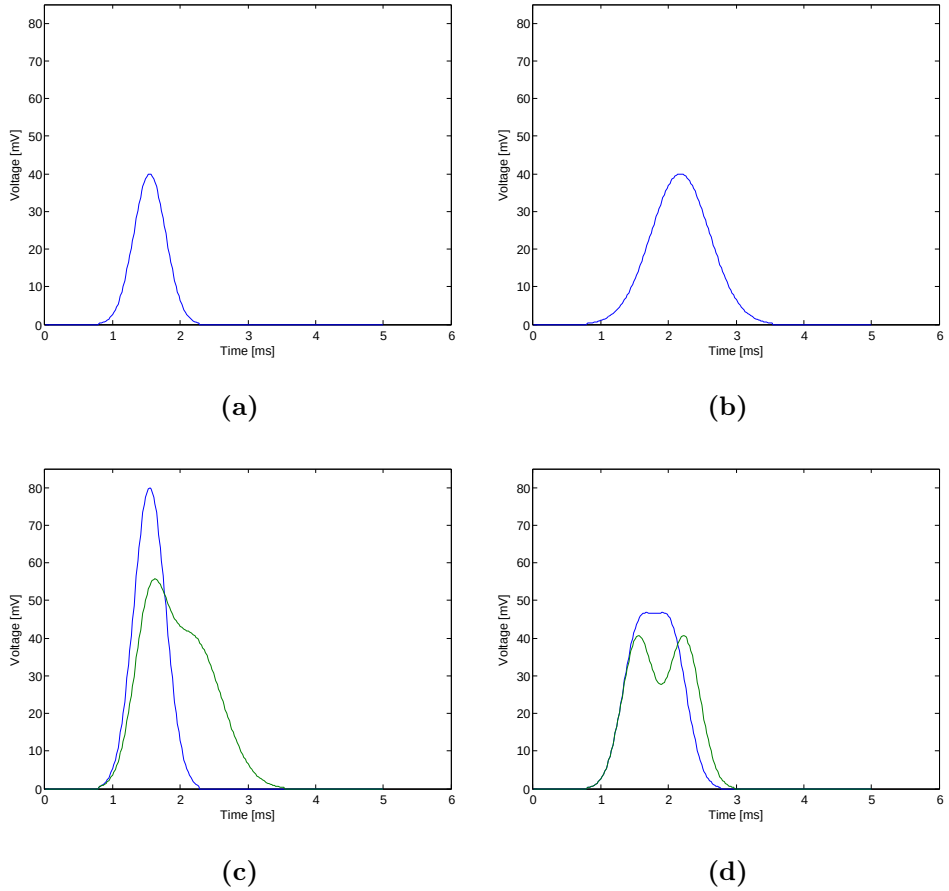

Figure 4: **(a)** Simulations of an action potential (without hyperolarization), c.f. Figure 2, using a Gaussian windowed sinusoid with peak value 40 mV and width at half maximum 0.5545 ms. **(b)** The same type of simulation, with peak 40 mV, but width at half maximum 1.0196 ms. **(c)** In blue, the sum of two potentials from (a). In green the sum of one potential in (a) and one in (b). **(d)** In blue, the sum of a potential in (a) and an identical such potential shifted +0.4883 ms. In green the sum of a potential from (a) and an identical such potential shifted +0.6836 ms. It appears that neurons that fire in parallell will give rise to different frequencies, and indeed number of frequencies, dependent on their synchronization as well as with dissimilarity in basic wavelengths.

Mentioned above are the seven features implemented with diagnostic objectives in mind. They are defined and accounted for in Section 2.2 and will, with various selection for each type of spectra, be applied to estimates of *power spectral density* (PSD), $S_x(f)$ and *time-frequency distribution* (TFD)

$W_z(t,f)$ from the 'signature' ABR of each person. This will be done separately for each cerebral hemisphere. In addition, we shall consider features of the *cross power spectral density* (CPSD), $\Gamma_{x_1x_2}(f)$, between the hemispherical channels, making it possible to quantify the simultaneousness, i.e. the phase-shift, and the equivalence in spectral content between the brain-halves. When referring to the feature space, *particularly in figure captions*, this will assume the notation:

$$\Theta_{M,\Lambda,\varphi,\xi,h}. \tag{1.1}$$

Here, type of feature $\varphi = \{\mathcal{H}_1, \mathcal{H}_2, \mathcal{I}, \mathcal{K}, \mathcal{E}_1, \mathcal{E}_2, \mathcal{P}\}$ from estimation $\Lambda = \{\text{P,C,TF}\}$ (for PSD, CPSD, TFD) using data-treatment method $M = \{\text{win, b-p}\}$ (window and band-pass respectively), and cerebral hemisphere $h = \{\text{L,R,B}\}$, L for *Left*, R for *Right* and B for a *comparison between Both*. As for ξ, throughout this study this will signify either a test subject or a group of such with F for female, M for male, A for ADHD and C for healthy control. In the case of a specific test subject, a number will be added as the index within the group. Examples are $\xi = FA12$ for the 12^{th} female in the ADHD-group, $\xi = M$ for all males or $\xi = C$ for all persons in the control group.

When comparing features between disease-groups, data will be divided with respect to gender. There are three main reasons for this: *i)* There is a significant gender difference in skull size. In general, men have 10% larger skulls, while women's skulls are thicker [36], introducing possible biases in terms of signal strength or other characteristics. *ii)* In some aspects [37], [38], [39] there are confirmed gender differences also in cerebral functionality. *iii)* ADHD as a diagnosis is much more common [40] among boys/men, lending relevance to a gender division in any study of the disorder. For illustrative purposes, the course of action in this study is outlined graphically in Figure 5.
In evaluating the performance for each method and feature let

$$\begin{aligned} \mathcal{A} &= \Theta_{M,\Lambda,\varphi,FA,h}, \\ \mathcal{C} &= \Theta_{M,\Lambda,\varphi,FC,h} \end{aligned} \tag{1.2}$$

be the sets containing each persons value for a given method, feature and cerebral hemisphere in the female ADHD group ($\xi = FA$) and control ($\xi = FC$) groups respectively. It is hypothesized that for $\mathcal{A}$ and $\mathcal{C}$, and analogously for the corresponding male groups, the ADHD and control groups might differ, yielding hypotheses:

$$\begin{aligned} H_0 &: \ \eta^*_{\mathcal{A}} = \eta^*_{\mathcal{C}}, \\ H_1 &: \ \eta^*_{\mathcal{A}} \neq \eta^*_{\mathcal{C}}, \end{aligned} \tag{1.3}$$

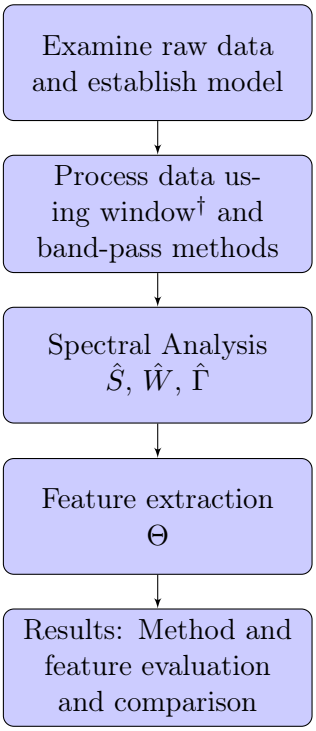

Figure 5: Flow chart describing the working stages of this study. $\hat{S}$, $\hat{W}$ and $\hat{\Gamma}$ are estimates of the PSD, TFD and CPSD respectively. Θ are the collection of spectral estimate features (Equation 1.1) to be extracted and evaluated. † - note that this method will also require selecting a sub set of the subject sample.

meaning that rejection of H_0 points in the direction that the given feature φ in cerebral hemisphere h using method M could serve as a relevant frequency-based trait for ADHD-diagnostics. Here, η^* is an estimation of the 'center of gravity', η, in a distribution of persons in disease group in a given feature. η^* will be estimated using the Wilcoxon rank-sum test[9], to be described in Section 3.3.1.

[9]Known in many applied sciences as the Mann-Whitney test.

2 Theory

The PSD, CPSD and TFD are the spectral representations used in this study. Section 2.1 below contains a presentation of the non-parametric estimators of the PSD, CPSD and TFD to be implemented for all subsequent purposes, [48]. This study is not aimed at finding 'best in show' estimates, hence Section 2.1 is purposefully brief and to the point. For a more thorough presentation of stationary processes, spectral estimation and time-frequency distributions, the reader is advised to consult [46], [48]. Rather than focusing on different methods of spectral estimation, our focus lies more in investigating the features, Θ, outlined in Section 1.5. The features, to be extracted from the PSD, CPSD and TFD, are accounted for in Section 2.2.

2.1 Spectral and Time-Frequency Analysis

Consider a sampled signal in discrete time:

$$x_i, \;\; i = 1...N \tag{2.1}$$

for some signal length N. First, let us make the assumption that x_i is an outcome of a stationary process, that is: it's mean and correlation function are independent of time i. Further, consider the power spectral density (PSD) estimate of x_i by means of a Hanning windowed periodogram, according to:

$$\hat{S}_x(f) = \frac{1}{N}\left|\sum_{k=1}^{N} x_k h_k \, e^{-i2\pi fk}\right|^2 \tag{2.2}$$

with

$$h(k) = 0.5\left(1 - \cos(\frac{2\pi k}{N-1})\right), \; k = 1...N. \tag{2.3}$$

As a second spectral representation, we shall consider the cross power spectral density (CPSD), a spectral measure of correlation between signals. Consider signals x, y as in 2.1. Now, let us form the cross-covariance estimate between these as:

$$\hat{r}_{x,y}(k) = \frac{1}{N}\sum_{t=k+1}^{N}(x_t - \hat{m}_x)(y_{t-k} - \hat{m}_y) \tag{2.4}$$

The CPSD may then be estimated as

$$\hat{\Gamma}_{x,y}(f) = \sum_{k=1}^{N} \hat{r}_{x,y}(k) e^{-i2\pi fk} \tag{2.5}$$

with $\hat{r}_{x,y}$ from Equation 2.4. In this study, the periodogram will be estimated for both cerebral hemispheres separately, thus representing the spectral content in each. The CPSD estimate of Equation 2.5, however, will be used to compare hemispheral correlation with x and y in $\hat{\Gamma}_{x,y}$ being the mean observational signals from a test subject's left and right cerebral hemispheres.

Apart from $\hat{S}_x(f)$ and $\hat{\Gamma}_x(f)$, we shall take on a non-stationary approach to spectral estimation, i.e. time frequency distributions (TFD:s). We shall utilize the so called windowed (or pseudo) Wigner-Ville distribution (WVD) seen in Equation 2.6 below. When computing TFD:s, one is advised always to transform the signal under consideration by means of the Hilbert transform, thus yielding an analytic (discrete) signal z_i for which $Z(f) = 0$ for $f < 0$ [48, ch.3.2]. In discrete time, any TFD is thus applied to a signal z_i. We may form the discrete WVD[49, p.235] as

$$\hat{W}_z(n,k) = 2 \sum_{|m|<M/2} g_m \; z_{n+m} \; z^*_{n-m} \, e^{-i2\pi mk/M}, \tag{2.6}$$

where we will use $M = N/10$ and N as before is the signal length, z_i is the analytic signal, $n = 1...N$ and $m \in \mathbb{Z}$. The function g is a so called doppler-independent kernel, and will take on the form of a Hanning window according to:

$$g_j = \begin{cases} \tilde{h}(j) & \text{if } |j| < M/2 \\ 0 & \text{otherwise,} \end{cases} \tag{2.7}$$

with $\tilde{h}(j)$ is a Hanning window as in Equation 2.3, but centered at zero and with length M instead of N, and $j \in \mathbb{Z}$. $\hat{W}_z$ is the TFD-estimation from which certain features, described below, are to be extracted.

2.2 Features of Spectral Estimates

Concentration measures are *features* of a given distribution, theoretical or empirical, and a common way to describe its dispersion or shape. For instance, some well known such measures from the field of statistical inference are[10] the variance, skewness and kurtosis. Far from being limited to these quantities, any moment or function thereof can serve as a feature and may well reveal and describe some property of given data or a distribution function. Spectral estimations, examples of which are seen above in Section 2.1, are indeed ways to describe frequency content or *distribution* in a given signal, and it is hypothesized that the features specified below are ways to capture possible differentiated and disease-specific neural synchronization as

[10]The mean, or expected value, is a measure commonly considered for data and theoretical distribution functions respectively. This does not, however, contain any information about *concentration* as such

outlines in Figure 4. The features chosen for this study are picked on merits of being well established in information theory or bioelectrical signal processing.

For a given spectral estimate $\hat{S}$ (or $\hat{\Gamma}$) we may define the n^{th} moment as

$$M_n = \int_{-\infty}^{\infty} f^n \hat{S}_x(f) df \tag{2.8}$$

Using combinations of such moments, we may define a set of measures commonly used in bioelectrical signal processing [50, p. 99-103]. Namely, the *Hjorth descriptors* and *spectral purity index*. The 0^{th} Hjorth descriptor

$$\mathcal{H}_0 = M_0. \tag{2.9}$$

, also called *activity*, is nothing but the first moment, or in the terminology of the correlation function we have $\mathcal{H}_0 = r_x(0)$, with the same x denoting an arbitrary signal as in 2.8. As we shall see, all PSD estimates to be derived will be *normalized*, hence $\mathcal{H}_0$ will be identical for all spectra and lack meaning for these. This is not true for the CPSD estimates, $\hat{\Gamma}$, where $\mathcal{H}_0$ will certainly be used and seen as a measure of total correspondence between hemispheres. The 1^{st} Hjorth descriptor is defined as the square root transformed ratio,

$$\mathcal{H}_1 = \sqrt{\frac{M_2}{M_0}}, \tag{2.10}$$

which is also called *mobility*, and is an estimate of the dominant frequency. Alternatively, one could say that $\mathcal{H}_1$ describes a *center of mass* in frequency. The 2^{nd} Hjorth descriptor,

$$\mathcal{H}_2 = \sqrt{\frac{M_4}{M_2} - \frac{M_2}{M_0}}, \tag{2.11}$$

is referred to as *complexity* and is an estimate of the spectral bandwidth. Alternatively, this may be seen as a variance measure in frequency. Finally, among the moment-based measures we have the spectral purity index,

$$\mathcal{I} = \frac{M_2^2}{M_4 M_0}. \tag{2.12}$$

The name reflects the fact that this measure conveys how 'well' data is modelled by a single sinusoid, with $\mathcal{I} = 1$ for a perfect such fit. Hence, it is suggested that $\mathcal{I}$ is also a measure on (lack of) complexity in the ABR-spectra, and is assumed to correlate negatively with $\mathcal{H}_2$.

As to adopt an alternative approach, independent of the moments in 2.8, consider the PSD or CPSD estimates from Equations 2.2, 2.5. Disregarding the peaks in the spectra, these estimates are typically monotone and

decreasing for the types of data here considered, with higher magnitude in lower frequencies. Applying a log-transform to $\hat{S}_x(f)$ renders this decrease sufficiently linear [50, p. 99], and a first degree polynomial function $h(f;\boldsymbol{\theta})$ may be fitted by:

$$\tilde{\boldsymbol{\theta}} = \arg\min_{\boldsymbol{\theta}} \int_{-\infty}^{\infty} (h(f;\boldsymbol{\theta}) - \log \hat{S}_x(f))^2 df. \tag{2.13}$$

Thus, $h(f,\tilde{\boldsymbol{\theta}}) = \tilde{\theta}_0 + \tilde{\theta}_1 f$ provides the best fit in a least-squares sense and the linear parameter is taken to be a feature describing, albeit rather crudely, the ratio between high and low frequencies present in the signal, i.e.

$$\mathcal{K} = \tilde{\theta}_1 \tag{2.14}$$

is the slope feature used in the continuation.

The two last features used for $\hat{S}$, and the only two used for $\hat{W}$, are renditions of *Rényi entropy* with two different parameter values. Entropy is a measure on *uncertainty* or *disparity*, i.e. higher entropy means, in this case, a more widespread spectrum.

Rényi entropy takes the following shapes for spectral estimates,

$$R_{\hat{S}}(\alpha) = \frac{1}{1-\alpha} \log_2 \left(\int_{-\infty}^{\infty} \hat{S}^{\alpha}(f)\, df \right) \tag{2.15}$$

and time-frequency distributions,

$$R_{\hat{W}}(\alpha) = \frac{1}{1-\alpha} \log_2 \left(\int_{t_0}^{t_N} \int_{-\infty}^{\infty} \hat{W}^{\alpha}(t,f)\, dtdf \right) \tag{2.16}$$

respectively. As features, we shall consider

$$\mathcal{E}_1 = \lim_{\alpha \to 1} R(\alpha) \tag{2.17}$$

and

$$\mathcal{E}_2 = R(2) \tag{2.18}$$

with R from Equation 2.15 or 2.16. $\mathcal{E}_1$ is the so called Shannon entropy, well-established as a measure of disparity or complexity in information theory and bioinformatics, e.g. [51], [52]. Since $\mathcal{E}_1$ and $\mathcal{E}_2$ are not normalized, as are $\mathcal{H}_1$, $\mathcal{H}_2$, $\mathcal{I}$, these will not be used for the un-normalized cross spectral estimate $\hat{\Gamma}$.

In summary, for the PSD estimate (Equation 2.2) we shall consider features $\mathcal{H}_1$, $\mathcal{H}_2$, $\mathcal{I}$, $\mathcal{K}$, $\mathcal{E}_1$, $\mathcal{E}_2$ for both hemispheres. For the CPSD estimate (Equation 2.5) we shall consider $\mathcal{H}_1$, $\mathcal{H}_2$, $\mathcal{I}$, $\mathcal{K}$ for the comparison between hemispheres, and for the TFD estimate we shall consider $\mathcal{E}_1$, $\mathcal{E}_2$ for both hemispheres.

2.2.1 Power in Frequency Bands – An Additional Feature

As work progressed, an additional feature was brought into consideration. This method is based on *power in frequency band*, common in biomedical signal procesing [50, p. 98-99]. This feature is treated as additional in the sense that it is to be used only for the band-pass method, and also for the fact that it is not completely impartial. Rather, it is conditioned on the findings of the spectral analysis. Power in frequency bands, to be labled $\mathcal{P}$, is simply:

$$\mathcal{P} = \frac{\int_{f_0}^{\infty} \hat{S}_x(f)df}{\int_{-\infty}^{\infty} \hat{S}_x(f)df}. \tag{2.19}$$

Here, two main approaches as to find the limit frequency f_0 may be adopted: *i)* An empirical approach, viewing spectra among the persons and estimating, roughly by inspection, a common break point between peaks. *ii)* Optimizing by, for instance, looking for best clustering properties (in our case between disease groups) with different choices of f_0. For simplicity, we shall choose option *i*, while choice of f_0 and the results in the feature spaces obtained by use of Equation 2.19 can be seen in Section 4.2.3.

3 Data and Methods

3.1 Hardware and Measurement

The ABR-measurements used in this study were carried out by personnel at SensoDetect[11] using their patented BERA[12]-system. The complete system is shown in Figure 6.

Figure 6: The BERA-equipment setup. The frontal electrodes of the two channels, left in black and right in yellow, are here seen. The corresponding opposite pole of each are located right behind each ear. The channels are attached to ground separately. The AD-conversion is performed with a resolution of $0,05$ mV using 16-bit hexadecimal conversion. Image source: [59].

The induced sound stimuli consist of square shaped pulses with duration 0.136 ms with a rise and fall time of 0.023 ms. The square shape characteristic means that the test subject will experience a short pulse, or 'click', of white noise[13]. The clicks used here come with an interstimulus interval from onset to onset of 0.192 ± 0.012 seconds. The variability between each click is assigned as drawn from a normal distribution, but each test subject is presented with the same 'stimulus train', i.e. 'soundtrack'. There are two

[11] SensoDetect AB is company which carries out statistical analysis with objectives similar to this study, namely to create reliable diagnostic tools for psychiatry. The company have previously focused research and product development on the aforementioned case of schizophrenia [28], and are currently distributing a solution for diagnostic support covering this disease.

[12] Brainstem Evoked Response Audiometry, another abbreviation for ABR

[13] i.e containing 'all frequencies'. This is only one of many sound profiles which has been used in ABR-applications, one may for instance consider different kinds of chirps [42] or an addition of masking sounds [28], [30].

main reasons behind this random shift in time. One is noise cancellation; with a varying interstimulus time, 'unwanted' neural activity of far lower frequency present in the recording as well as possible other artifacts ought to be reduced when applying averaging over the observations. The other reason is to inhibit habituation; the repetitiveness of an equidistant stimulus train could well affect the brainstem[14] in ways which produces unwanted habituation-related alterations in the ABR [28].

3.2 Test Subject Data

The collected data consists of measurements from 69 subjects divided into groups as in Table 1 below. In using the window method, Section 3.4, we shall consider a sub division of these subjects selected based on certain criteria. With the adoption of the band-pass method, all subjects are included in the study.

Group\Gender	Female	Male
Healthy controls	$n_{FC} = 19$ $\rho_{FC} = [26, 62]$ years $m_{FC} = 40$ $-$"$-$ $s_{FC} = 11.27$ $-$"$-$	$n_{MC} = 17$ $\rho_{MC} = [21, 65]$ years $m_{MC} = 43.81$ $-$"$-$ $s_{MC} = 12.69$ $-$"$-$
ADHD	$n_{FA} = 18$ $\rho_{FA} = [17, 52]$ years $m_{FA} = 28.44$ $-$"$-$ $s_{FA} = 12.81$ $-$"$-$	$n_{MA} = 15$ $\rho_{MA} = [16, 59]$ years $m_{MA} = 30.33$ $-$"$-$ $s_{MA} = 11.16$ $-$"$-$

Table 1: Here, n - number of subjects, ρ - age range, m - mean age, s - standard deviation in age, for each group. Concerning the age of test subjects, it should be noted that for two test subjects, one in each control group, the age is unknown to the author. This study, however, does not attempt to model for or capture any age dependency.

Each test subject included in the study has gone through the same procedure, with the exception of some variation in the exposure time. For most subjects, measurement consists of around 2750 observations, 1375 on each side. Each observation includes 15 ms of recorded brainstem activity, made up of 256 samples equalling a sampling rate of $f_s \simeq 17$ kHz. It is of interest to make each persons ABR-recording fully comparable[15]. With this in mind, every

[14]The individual degree of habituation may very well be a trait worthy of study, but for our purposes we wish to be able to consider the individual ABR-observations to come from as similar a neural process as possible

[15]We may not want to compare cerebral activity which for some reasons tends to appear after recording times not reached during measurement on all test subjects

persons recording will be cut as to match the length of the shortest recording. This was for $\xi = MC16$ and consisted of 2478 observations. Measurements are taken on each side of the brain and these two hemisphereal channels will in all following analysis be considered separately. We may then form two matrices:

$$\begin{aligned} x^L_{t,T}, \;\; t = 1...N, \;\; T = 1...M, \\ x^R_{t,T}, \;\; t = 1...N, \;\; T = 1...M, \end{aligned} \tag{3.1}$$

containing the recorded raw data for the left and right hemisphere respectively. Here, t is the intra-observational time and T the observation number and $N = 256$, $M = 2478/2 = 1239$. In the following, when talking about a given observation from either hemisphere, i.e. a column in $x_{t,T}$ from Equation 3.1, this will be denoted

$$x_t, \;\; t = 1...N. \tag{3.2}$$

Examining the raw data is a natural first step, and is aimed at discovering occurrence and characteristics of artifacts, 'broken' samples and other anomalies in the data. In Figure 7 below, the mean observation in raw data for persons $\xi = MA4, FA11, FC9$ are seen.
Figure 7 shows artifacts of various types occurrent in the data, which are to be dealt with by processing the signal. i To follow in Section 3.3 are the assumptions made for the purpose of modelling and treating data.

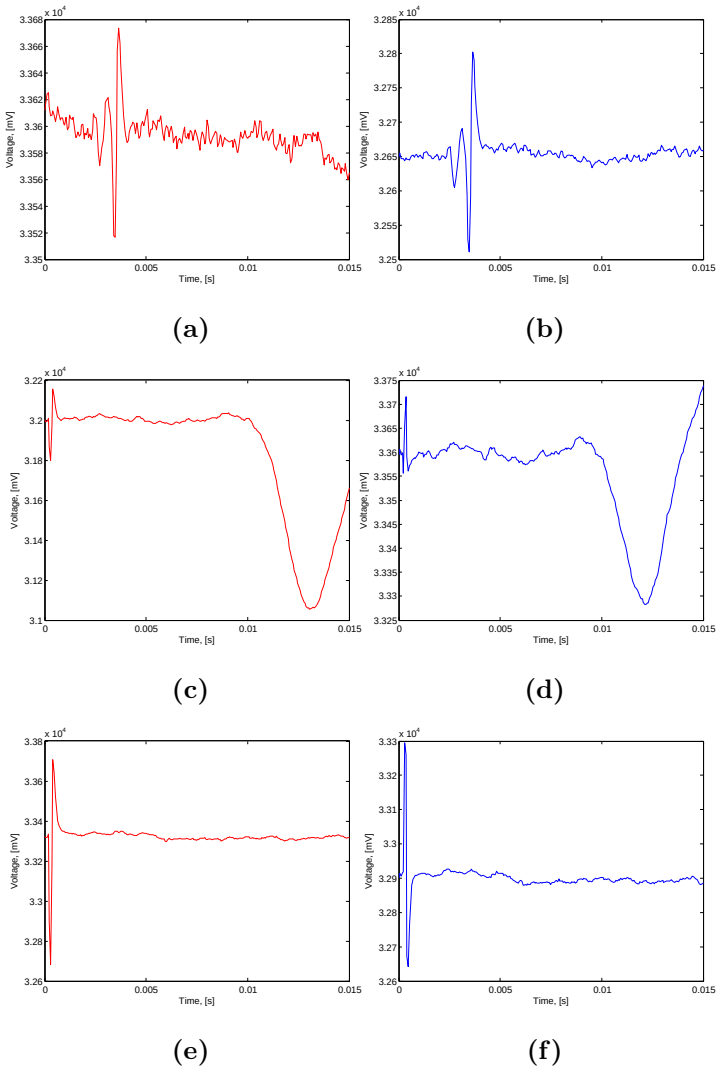

Figure 7: Mean observations from raw data and 3 persons. (a) and (b) are from person $MA4$, left and right hemispheres respectively. (c) and (d) are left and right hemisphere mean observations from person $FA11$. Finally (e) and (f) come from person $FC9$, left and right hemisphere.

3.3 Model for Data

In all following analysis, based on examination of the raw data, it is assumed that no trend in the global time T of observation number can be seen. That is, we regard the ABR to be suffiently deterministic and identical between observations. As mentioned in 1.4, this is the common way to regard any kind of ERP:s. The variability between observations is thus considered to arise from noise assumed to be independent to the brainstem activity. This noise will typically be of the following origins: *i)* The 'EEG': That is, lower frequency modulations coming from all other cerebral activity but the ABR as picked up by the electrodes. *ii)* Muscular noise from cranial and ocular muscles contracting and relaxing throughout the recording procedure. *iii)* Hardware disturbances from the equipment and power-lines, the familiar 50/60 Hz will here be examined. *iv)* Electrode motion artifacts: disturbances arising from movements of the electrodes or variations in connectivity with the skin.

As mentioned in Section 1.4, ABR:s are commonly assumed to be identical between observations. The variation between observations is therefore considered to spring from the noise as described above. In all, we assume the underlying ABR to be constant in global time T, we may model a given observation with:

$$x_t = v_t + \epsilon_t, \tag{3.3}$$

where ϵ_t is the noise in the particular observation stemming from physical and technical sources mentioned above. For the reason mentioned above in 3.1, that the inter-stimulus time interval is varied, ϵ_t is assumed to be iid[16]. Further, v_t in Equation 3.3 is the assumed 'true', or *characteristic, individual ABR we wish to capture and study.* We can conclude that if we consider a zero-mean signal and with the assumption of a v_t constant in observational time T, i.e. $V(v_t) = 0$ then.

$$\begin{aligned} D(x_t) &= D(\epsilon_t) \\ &\Rightarrow \\ D(\bar{x}_{t,T}) &= \frac{D(\epsilon_t)}{\sqrt{M}}. \end{aligned} \tag{3.4}$$

With V and D being the variance and standard deviation respectively. As we shall see, the number of observations M available for each person is $M \simeq 1200 \Leftrightarrow \sqrt{M} \simeq 35$. For all practical purposes, it is assumed that with the model in Equation 3.3 and the averaging over (assumed) iid noise ϵ_t in Equation 3.4, the noise is sufficiently reduced. That is, we expect to obtain

[16] identically and independently (between observations) distributed

the characteristic ABR by taking the mean over all observations, i.e. for left and right hemispheres, the mean observations

$$\begin{array}{ll} \bar{x}_t^L, & t = 1...N, \\ \bar{x}_t^R, & t = 1...N \end{array} \tag{3.5}$$

are the quantities from which we wish to make spectral estimates; Equations 2.2, 2.5, 2.6.

It is thus established that we shall consider the mean hemispheral observations, $\bar{x}^L$, $\bar{x}^R$, as the characteristic ABR-responses from each person. The two data pre-processing methods, the window method and the band-pass method, are presented in Sections 3.4 and 3.5 respectively. These are to be applied to each observation of data prior to forming the means in Equation 3.5. Before describing these methods, a brief word on the statistical testing used to study significance between disease-groups in feature spaces follows in Section 3.3.1.

3.3.1 Statistical Testing: Wilcoxon rank-sum test

When comparing groups with the objective of finding significant inter-group differences, c.f. Equation 1.3, we shall utilize the *Wilcoxon rank-sum test*[58],[47, p.121]. This test makes no assumption about normality, which is particularly appropriate with relatively small data sets[17] that appear not to be normally distributed. The test does however demand that compared data comes from distributions of equal variance. For the purpose of this study, we shall assume that any outcomes of features from an ADHD-group and a control group respectively are indeed equal in variance[18].

The (doble-sided) Wilcoxon rank-sum test operates in the following fashion: Consider two *ranked*, i.e. sorted in order of magnitude, data sets ω_i, λ_j, $i = 1...n$, $j = 1...m$, $n \neq m$ whose means are to be tested with a hypothesis such as Equation 1.3 in mind. Consider further a quantity T defined as:

$$T = \sum_{i=1}^{n} (\#\ of\ values\ in\ \lambda_j\ smaller\ than\ \omega_i). \tag{3.6}$$

Now, we define U as:

$$U = n \cdot m + \frac{n \cdot n + 1}{2} - T. \tag{3.7}$$

[17] As we shall see, the smallest disease-gender-group will be as small as 7 using the window method, and 15 using the band-pass mathod.

[18] Certainly, we could here utilize some form of analysis of variance (ANOVA), however an assumption of equal variance is common practise in dealing with this form of human individual measurement, and the reader is kindly asked to hold this to be true.

Under certain conditions[19] U is normally distributed with expected value and variance:

$$U \sim \mathcal{N}\left(\frac{n \cdot m}{2}, \frac{n \cdot m \cdot (n+m+1)}{12}\right). \tag{3.8}$$

Thus, from the assumption of normality, Equation 3.8, we may construct and use a test statistic $z \sim \mathcal{N}(0,1)$ according to.

$$z = \frac{\left(U - \frac{n \cdot m}{2}\right)}{\sqrt{\frac{n \cdot m \cdot (n+m+1)}{12}}}. \tag{3.9}$$

In turn, z may be subject to a standard two-sided t-test, which constitutes the last step in the procedure of the Wilcoxon rank-sum test. Being that this test considers ranks, comparison with this test does not say anything about whether *mean* values between groups may differ, but rather whether their *medians* do. i.e., the median is the 'center of gravity', η, mentioned in 1.3. However, under the assumption that the distributions of disease-group feature outcomes are symmetrically distributed, which is feasible, the mean and median are equal.

3.4 Window Method

As this algorithm for data pre-treatment here is highly specific for the study at hand, no in-depth theory is included[20]. Instead, each data treatment step is here accounted for independent of any derivations.

As to make data, as demonstrated in Figure 7, more apt for spectral estimation, the following steps of signal pre-processing were employed.

Step 1 Firstly, there is good reason to omit some samples from the beginning of the measurement. Test subjects here tend to react very differently in the habituation process, i.e. when getting used to the click-sound exposure [28]. Thus, the 50 first observations from each cerebral hemisphere are withdrawn from any further analysis

Step 2 Let x_t be a given ABR-observation, i.e. column in $x_{t,T}$ of length $N = 256$. As a first observation-wise procedure, we try to mitigate the apparent artifactal spikes seen for all test subjects in Figure 7. This

[19] Requirements are, loosely, n, $m > 20$. As we shall see, this demand not met using the window method (as this entails a sub selection of the subject sample), but almost with the complete subject sample used with the band-pass method

[20] A more rigorous, and introductory, account of signal processing is given in for instance [45].

is done by employing a median value window of length 11 which, for a given observation yields

$$\hat{x}_i = \text{med}([x_{i-5} \ \ldots \ x_{i+5}]), \ i = 6 \ldots N-5. \tag{3.10}$$

Step 3 Since we are at most interested in wavelengths up to 1 ms it is of clear interest to reduce high frequency noise, some of which is introduced by the median window[21], and some of which may be attributed to AD-resolution round-off errors. In order to obtain a smoother signal, we use a mean value window of length 7, i.e.

$$\tilde{\hat{x}}_i = \text{mean}([\hat{x}_{i-3} \ \ldots \ \hat{x}_{i+3}]), \ i = 4 \ldots N-3. \tag{3.11}$$

Step 4 As to remove any 'DC-level' from subsequent spectral estimation, mean values are subtracted from each corresponding observation, i.e.

$$\tilde{\hat{x}}_t = \tilde{\hat{x}}_t - mean(\tilde{\hat{x}}_t) \tag{3.12}$$

Step 5 Lastly, in wanting the characteristic ABR of a person we normalize all observations to contain the same energy, i.e. we normalize such that,

$$\sum_{i=1}^{N} \tilde{\hat{x}}_i^2 = N. \tag{3.13}$$

The interpretation of characteristic ABR employed here is thus that we let spectral content of observations contribute equally and not in proportion to energy within the observation.

As a comparison with Figure 7, these three observations can now be seen, filtered, in Figure 8.

As seen in Figure 8, the window method is unable to take care of low unwanted frequencies. In Figure 8, these are marked by possible prominent EEG disturbances or power line noise (c,d) and possible early onset cognitive responses (e,f). Based on this fact, a subset was selected for usage with the window method from the subject sample in 1. In this subset, subjects are selected only if they do not exhibit the low frequency noise as seen in Figure 8 (c,d,e,f). This new subject sample set can be seen in Table 2 below. Using these persons, we form the mean observation according to Equation 3.5. Having done this, we form the spectral estimates from Equations 2.2 (PSD), 2.5 (CPSD), 2.6 (TFD). Here, $\hat{S}_x(f)$ and $\hat{W}_z(t,f)$ are normalized, i.e. the reassignments

[21] As this samples from existing values

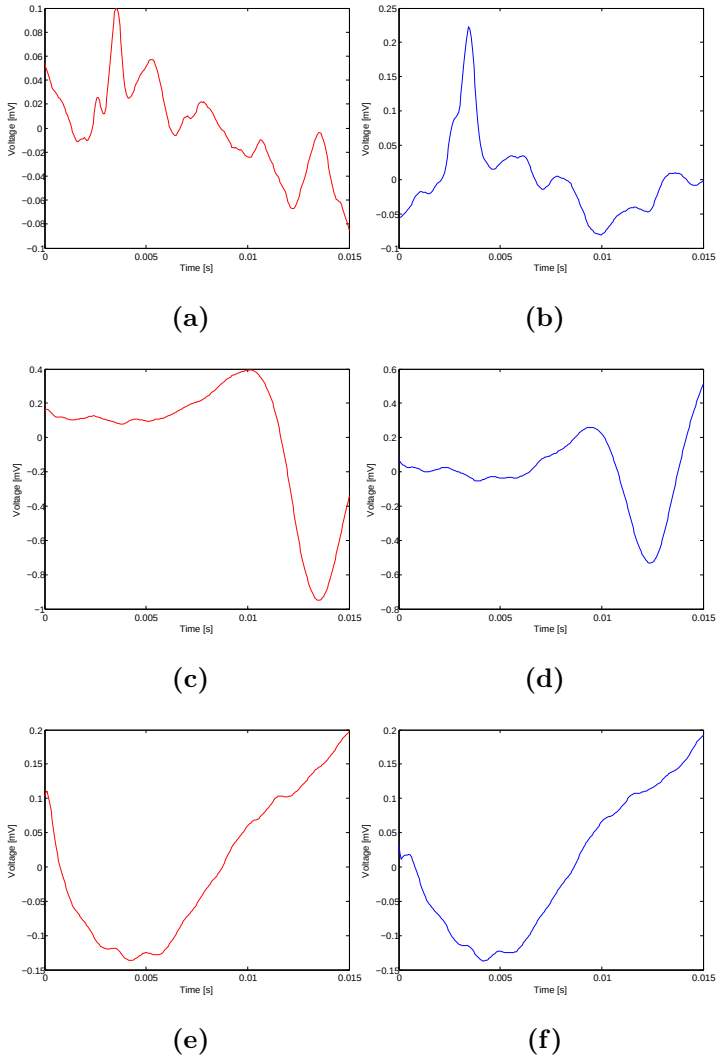

Figure 8: Mean observation in data filtetred by the window method from the same 3 persons as in Figure 7, $MA4$ (Left hemisphere in (a), right hemisphere in (b)) $FA11$ (Left hemisphere in (c), right hemisphere in (d)) and $FC9$ (Left hemisphere in (e), right hemisphere in (f)). It appears that there are possible early onset cognitive EEG in (c) and (d), as well as some low frequency disturbance in (e), (f) which are not properly filtered by the window method here used.

$$\begin{aligned} \hat{S}_x^n(f) &= \frac{\hat{S}_x(f)}{\int_{-\infty}^{\infty} \hat{S}_x(f)df} \\ \hat{W}_x^n(t,f) &= \frac{\hat{W}_z(t,f)}{\int_{-\infty}^{\infty}\int_{-\infty}^{\infty} \hat{W}_z(t,f)dfdt} \end{aligned} \tag{3.14}$$

Group\Gender	Female	Male
Healthy controls	$n_{FCS} = 10$ $\rho_{FCS} = [27, 62]$ years $m_{FCS} = 41.55 - "-$ $s_{FCS} = 12.34 - "-$	$n_{MCS} = 7$ $\rho_{MCs} = [21, 60]$ years $m_{MCS} = 37.14 - "-$ $s_{MCS} = 13.42 - "-$
ADHD	$n_{FAS} = 9$ $\rho_{FAS} = [17, 52]$ years $m_{FAS} = 27.55 - "-$ $s_{FAS} = 13.14 - "-$	$n_{MAS} = 7$ $\rho_{MAS} = [16, 59]$ years $m_{MAS} = 32.14 - "-$ $s_{MAS} = 14.48 - "-$

Table 2: The selected subject sample for which the window method is used. These are chosen on basis of not showing the characteristics of Figure 8 (c,d,e,f). As before, n - number of subjects, ρ - age range, m - mean age, s - standard deviation in age, for each group, with indexation denoting F - female, M - male, C - healthy control, A - ADHD. S denotes belonging to the selected subject sample.

are applied. This is not done for $\hat{\Gamma}$ as we wish to study the magnitude of the CPSD; the magnitude of correlation between brain hemispheres measured here by $\mathcal{H}_0$.

Having established the subject sample, features from Section 2.2 are applied to estimates, and results of feature performance with the window method are seen in Section 4.1.

3.5 Band-Pass Method

The window method algorithm developed above was intra-observational and designed with the characteristics of the raw data in mind, the method was also limited in the sense that a sub-selection of subjects (2) had to be made.

As a second method, we shall consider an approach, described below in steps, including the familiar linear band-pass filter. The steps of this method are outlined below.

Step 1 For the same reason mentioned in the Steps of 3.4 of wanting to cut observations from the beginning of the the recording, 50 observations from either side, $x^L_{t,T}$,$x^R_{t,T}$ are withdrawn. Also, each observation has 16 samples from the beginning and 41 samples from the end cut off. These limits are chosen empirically and aimed at capturing the 'worst' of early spike artifacts and higher cognitive responses showing up at the end of some persons observations. This yields observations now of length 200 samples, or 11.7 ms.

Step 2 The matrices containing observations on each side are converted into vectors, with each observation following the next. For this all-observation vectors, a linear band-pass filter with 3 dB cutoff frequencies $\mathbf{f} = [250,\ 1000]$ Hz and length 1000 in *global sample time* u, i.e. a time of length $t \cdot T$ covering all observations, was applied. This was to mitigate both high frequency artifacts and the lower frequency 'EEG'-noise from extra-brainstem activity.

Step 3 Due to filtering deterioration at the beginning and end of the all-observational vector, 5 observations $\simeq$ 1000 samples are withdrawn from each of $x^L_{t,T}$,$x^R_{t,T}$.

Step 4 The same procedures of de-meaning and energy-normalization as Steps 4, 5 in 3.4 are undertaken.

Just like with the window method, the mean observations, $\bar{x}^L_{t,T}$,$\bar{x}^R_{t,T}$, are produced, examples of which are seen in Figure 9 below, and estimates PSD, CPSD, TFD computed. Also as with the window method, the PSD and TFD estimates are normalized according to Equation 3.14. The performance of features produced from these estimates are found in Section 4.2.

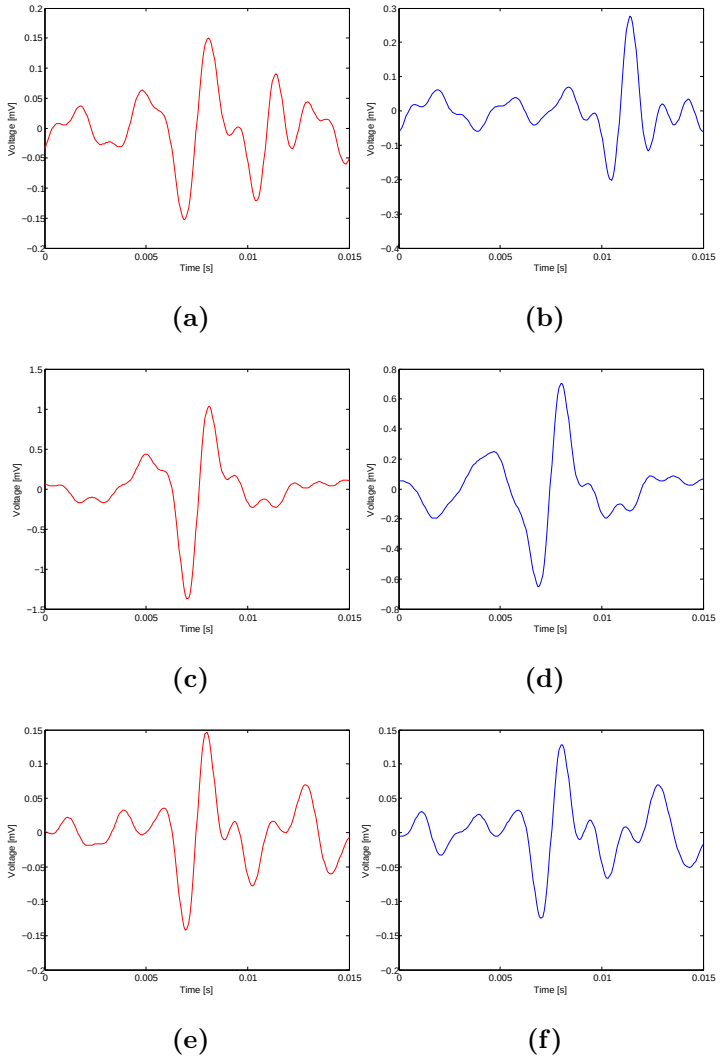

Figure 9: Mean observation in data filtetred by the window method from the same 3 persons as in Figure 7, $MA4$ (Left hemisphere in (a), right hemisphere in (b)) $FA11$ (Left hemisphere in (c), right hemisphere in (d)) and $FC9$ (Left hemisphere in (e), right hemisphere in (f)). It appears that the problems not dealt with by means of the window method are here mitigated by the band-pass method. It also appears that although we can make no claims on an exact number of peaks present, this treated data certainly resembles an 'idealized' ABR as shwon in Figure 3

,

4 Results

Some examples of the spectral estimates with basis in the window and band-pass methods are presented in Sections 4.1.1 and 4.2.1, while results of the feature analysis are found in Sections 4.1.2 and 4.2.2. These results consist of Tables 4 to 14 encompassing the p-values, i.e. the feature performance in distinguishing between disease groups, using all methods and features. Plots of how subjects fall out in certain features are presented in Sections 4.1.2 and 4.2.2 whenever significance is reached between disease groups, or when there are other reasons to look more closely at the feature performance graphically. However, as we shall see, no such plots are presented for the window method, as there is very little of interest in this respect.

Throughout all graphical representaions, blue circles (**o**) will denote control subjects and red crosses (+) those diagnosed with ADHD. Section 4.3 includes some analysis of how outcome between some features correlate, while Section 4.4 uses the significant results found for a brief endeavour into classification. Section 4.2.3 presents results from the 'additional feature', power in frequency bands ($\mathcal{P}$).

4.1 Window Method

4.1.1 Spectral Estimates

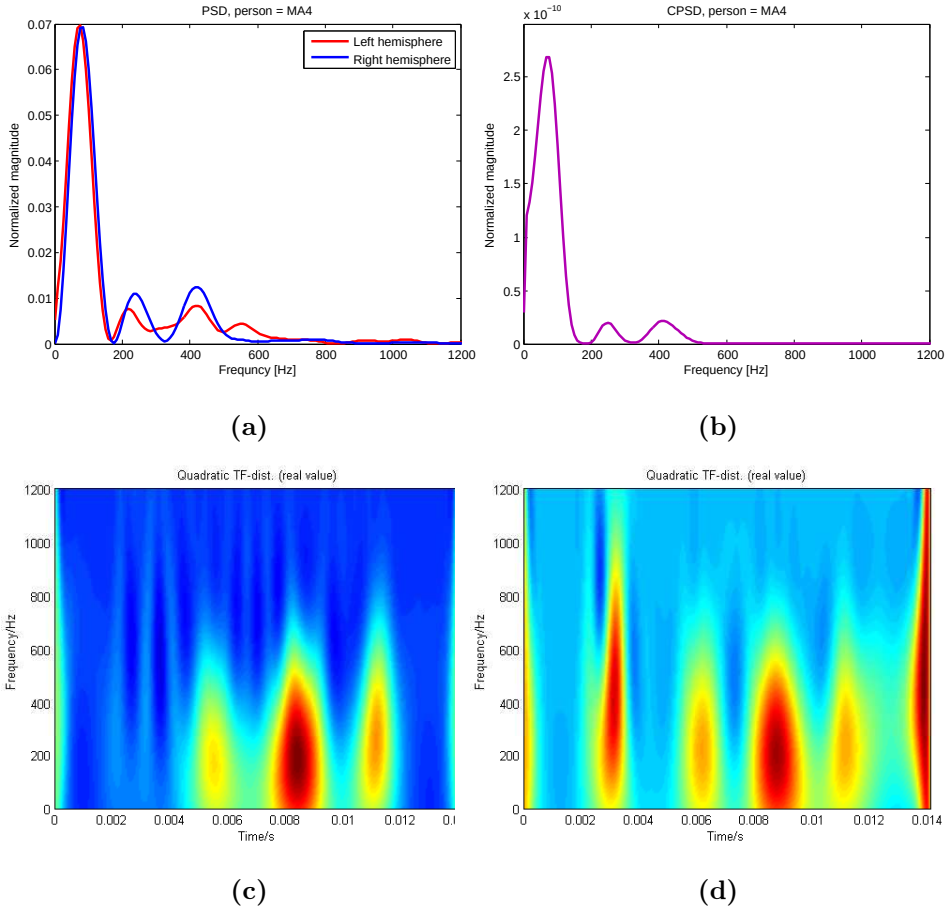

Figure 10: Figures showing spectras estimation from mean observations obtained using the window method shown in Figure 8 (a) and (b), i.e from person $MA4$. In the present figure, **(a)** are the left- and right hemisphere PSD:s, **(b)** is the CPSD between hemispheres. **(c)** and **(d)** are the left- and right hemisphere TFD:s respectively. It should be noted from all these plots that a considerable amount of low-frequency 'noise' is present, as the method used was not designed to deal with this problem in mind.

4.1.2 Feature Performance

Tables 3 and 4 below shows the performance of features obtained via the window method and PSD estimate for females and males respectively. No significance was found between disease groups, and no plots are presented.

Feature & hemisphere	p	Significance
$\mathcal{H}_1$, $Left$	0.5490	-
$\mathcal{H}_1$, $Right$	0.0535	-
$\mathcal{H}_2$, $Left$	0.7197	-
$\mathcal{H}_2$, $Right$	0.6607	-
$\mathcal{I}$, $Left$	0.7802	-
$\mathcal{I}$, $Right$	0.2110	-
$\mathcal{K}$, $Left$	0.1823	-
$\mathcal{K}$, $Right$	0.0535	-
$\mathcal{E}_1$, $Left$	0.8421	-
$\mathcal{E}_1$, $Right$	0.1564	-
$\mathcal{E}_2$, $Left$	0.9048	-
$\mathcal{E}_2$, $Right$	0.1564	-

Table 3: Feature performance using the window method and PSD estimate, females. No significant disease-group difference was found.

Feature & hemisphere	p	Significance
$\mathcal{H}_1$, $Left$	0.6200	-
$\mathcal{H}_1$, $Right$	0.4557	-
$\mathcal{H}_2$, $Left$	0.9015	-
$\mathcal{H}_2$, $Right$	0.9015	-
$\mathcal{I}$, $Left$	0.3829	-
$\mathcal{I}$, $Right$	0.3829	-
$\mathcal{K}$, $Left$	0.1649	-
$\mathcal{K}$, $Right$	0.3176	-
$\mathcal{E}_1$, $Left$	0.2086	-
$\mathcal{E}_1$, $Right$	0.9015	-
$\mathcal{E}_2$, $Left$	0.2086	-
$\mathcal{E}_2$, $Right$	0.7104	-

Table 4: Feature performance using the window method and PSD estimate, males. No significant disease-group difference was found.

For the cross spectral estimates estimates, Tables 5 and 6 show feature performance from features of CPSD for females and males respectively. As with the case of PSD, no significance was attained and no plots are shown.

Feature	p	Significance
$\mathcal{H}_0$	0.3562	-
$\mathcal{H}_1$	0.7197	-
$\mathcal{H}_2$	0.4967	-
$\mathcal{I}$	0.3562	-
$\mathcal{K}$	0.3154	-

Table 5: Feature performance using the window method and CPSD estimate, females. No significant disease-group difference was found.

Feature	p	Significance
$\mathcal{H}_0$	0.2086	-
$\mathcal{H}_1$	0.7104	-
$\mathcal{H}_2$	0.5350	-
$\mathcal{I}$	0.7104	-
$\mathcal{K}$	0.4557	-

Table 6: Feature performance using the window method and CPSD estimate, males. No significant disease-group difference was found.

Lastly, in Tables 7, 8, follow the results using TFD for females and males respectively.

Feature & Hemisphere	p	Significance
$\mathcal{E}_1$, $Left$	0.8421	-
$\mathcal{E}_1$, $Right$	0.0789	-
$\mathcal{E}_2$, $Left$	0.8421	-
$\mathcal{E}_2$, $Right$	0.0653	-

Table 7: Feature performance using the window method and TF estimate, females. No significant disease-group difference was found.

Feature & Hemisphere	p	Significance
$\mathcal{E}_1,\ Left$	0.8048	-
$\mathcal{E}_1,\ Right$	0.9015	-
$\mathcal{E}_2,\ Left$	0.8048	-
$\mathcal{E}_2,\ Right$	0.9015	-

Table 8: Features performance using the window method and TF estimate, males. No significant disease-group difference was found.

4.2 Band-Pass Method

4.2.1 Spectral Estimates

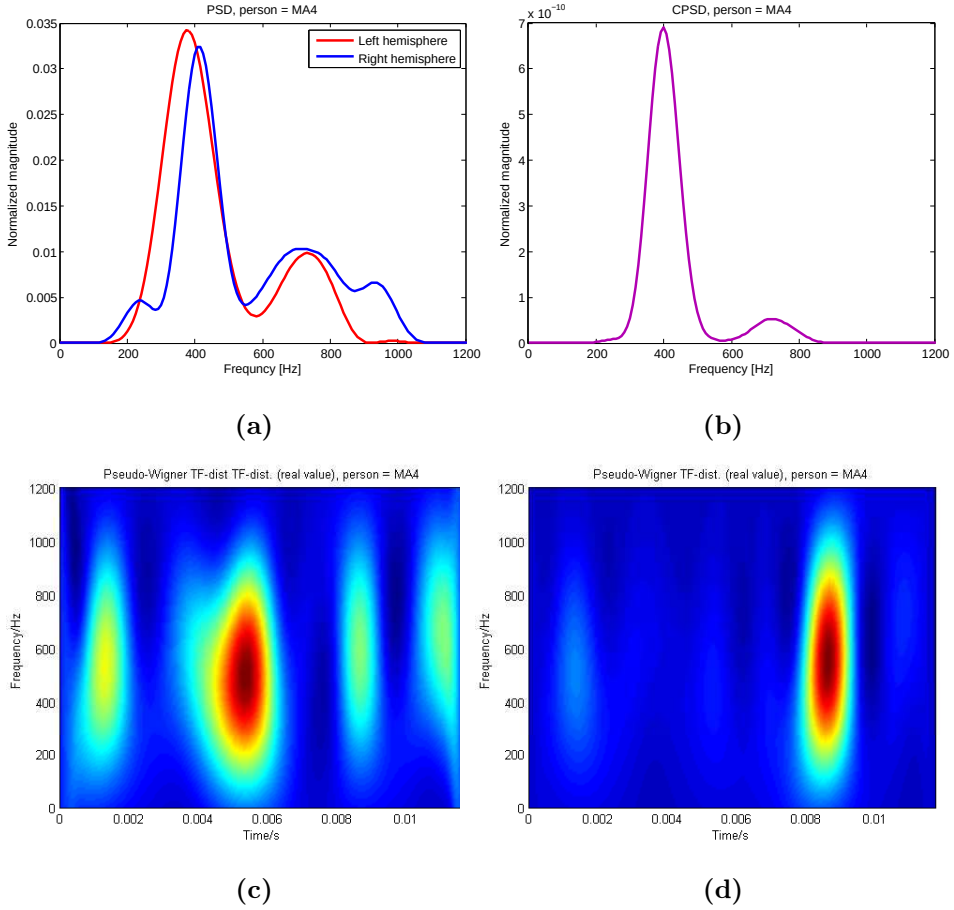

Figure 11: Figures showing spectral estimates from mean observations shown in (a) and (b) of Figure 9. The figure here at hand shows: **(a)** the left- (red) and right (blue) hemisphere PSD:s, **(b)** is the CPSD between hemispheres. **(c)** and **(d)** are the left- and right hemisphere TFD:s respectively.

Figure 11 shows spectral estimates from $\xi = MA4$. It is interesting to note that there seems to be no significant time-dependency of the frequency in (c) and (d), thus we may conclude that working under the assumption that the ABR is stationary is valid for, at least, this person. Other individual's TFD:s tell the same tale. Compared to 10, it is evident that the band-pass filtering has done its job: no low frequencies remain. It is also interesting to note, in the PSD and CPSD, that one peak has been 'lost' as compared to the window method.

4.2.2 Feature Performance

Using the band-pass method, consider first Table 9 below with the female group and PSD estimate. Here, certain significant disease-group differences were found. Consider results of $\mathcal{H}_1$ in Figure 12 and $\mathcal{H}_2$, Figure 13, below. Comparing results in these figures, it could be argued that the ADHD group has more content in the lower frequency range, affecting *both* dominant frequency and bandwidth.

Table 10 shows the PSD features in the male group. Here, no significance was reached and no graphic result is shown. Moving over to the CPSD, p–values as given by Table were found for the female group, Table 11, and make group, 12 respectively. Here, no significance was achieved, but we shall take a closer look at the $\mathcal{H}_0$ feature in the male group, Figure 14. The results from the TFD are seen tables 13 and 14. Here, no significant disease group difference is seen or presented.

Feature & Hemisphere	p	Significance
$\mathcal{H}_1$, $Left$	**0.0276**	*
$\mathcal{H}_1$, $Right$	0.1489	-
$\mathcal{H}_2$, $Left$	**0.0009**	****
$\mathcal{H}_2$, $Right$	0.9879	-
$\mathcal{I}$, $Left$	**0.0028**	***
$\mathcal{I}$, $Right$	0.4384	-
$\mathcal{K}$, $Left$	0.3540	-
$\mathcal{K}$, $Right$	**0.0322**	*
$\mathcal{E}_1$, $Left$	0.5333	-
$\mathcal{E}_1$, $Right$	0.8912	-
$\mathcal{E}_2$, $Left$	0.4566	-
$\mathcal{E}_2$, $Right$	0.9394	-

Table 9: Features performance using the band-pass method and PSD estimate, females. Significant disease-group difference found using $\mathcal{H}_1$ on left hemisphere (*), $\mathcal{H}_2$ on left hemisphere (****), $\mathcal{I}$ on left hemisphere (***) and $\mathcal{K}$ for the right hemisphere (*).

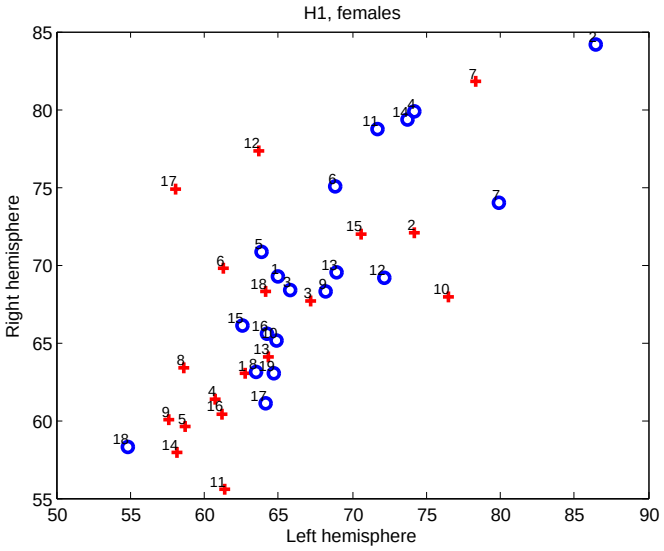

Figure 12: $\Theta_{b-p,PSD,\mathcal{H}_1,F,L}$ against $\Theta_{b-p,PSD,\mathcal{H}_1,F,R}$. ADHD in red, controls in blue. $p = 0.0276$ for this feature for the left hemisphere mean observation. It appears that the ADHD group has a significantly (***) lower dominant frequency on the left side ABR.

Feature & Hemisphere	p	Significance
$\mathcal{H}_1,\ Left$	0.4967	-
$\mathcal{H}_1,\ Right$	0.5457	-
$\mathcal{H}_2,\ Left$	0.2269	-
$\mathcal{H}_2,\ Right$	0.1740	-
$\mathcal{I},\ Left$	0.1623	-
$\mathcal{I},\ Right$	0.5970	-
$\mathcal{K},\ Left$	0.1863	-
$\mathcal{K},\ Right$	0.5209	-
$\mathcal{E}_1,\ Left$	0.5209	-
$\mathcal{E}_1,\ Right$	0.3079	-
$\mathcal{E}_2,\ Left$	0.5209	-
$\mathcal{E}_2,\ Right$	0.2573	-

Table 10: Feature performance using the band-pass method and PSD estimate, males. No significant disease-group difference was found.

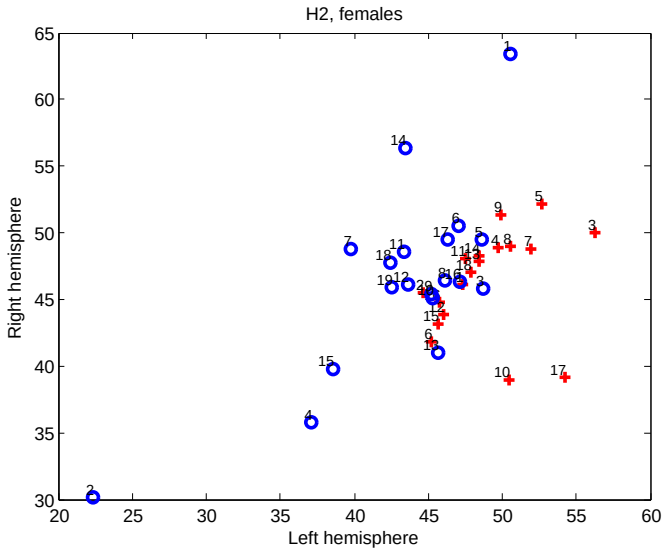

Figure 13: $\Theta_{b-p,PSD,\mathcal{H}_2,F,L}$ against $\Theta_{b-p,PSD,\mathcal{H}_2,F,R}$. ADHD in red, controls in blue. $p = 0.0009$ or this feature for the left hemisphere mean observation. It appears that the ADHD group has significantly (****) larger bandwidth on the left side.

Feature	p	Significance
$\mathcal{H}_0$	0.6595	-
$\mathcal{H}_1$	0.3087	-
$\mathcal{H}_2$	0.6161	-
$\mathcal{I}$	0.4384	-
$\mathcal{K}$	0.8673	-

Table 11: Feature performance using the band-pass method and CPSD estimate, females. No significant disease-group difference was found.

Feature	p	Significance
$\mathcal{H}_0$	0.1740	-
$\mathcal{H}_1$	0.5209	-
$\mathcal{H}_2$	0.7340	-
$\mathcal{I}$	0.7340	-
$\mathcal{K}$	0.7057	-

Table 12: Feature performance using the band-pass method and CPSD estimate, males. No significant disease-group difference was found.

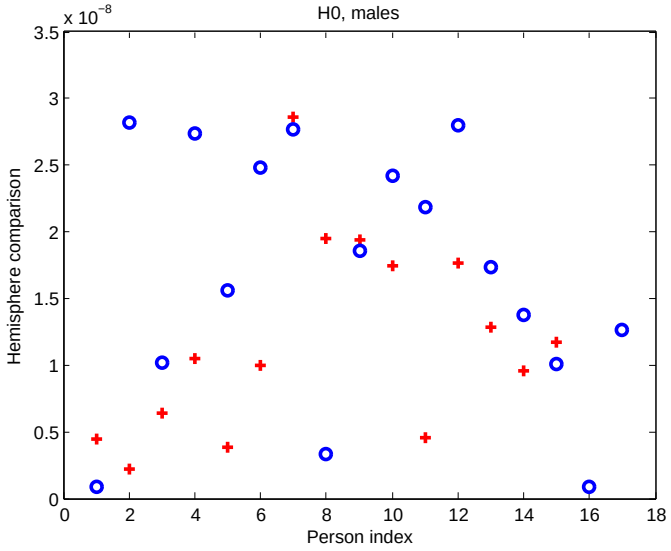

Figure 14: Person index within each group and their respective $\Theta_{b-p,CPSD,\mathcal{H}_0,M,B}$. ADHD in red, controls in blue. No statistical significance was achieved, but aside for a few outliers, a vague trend of ADHD subjects displaying lower hemispheral correlation, resulting in lower energy in the CPSD which is precisely $\mathcal{H}_0$, can be seen.

Feature & Hemisphere	p	Significance
$\mathcal{E}_1,\ Left$	0.2545	-
$\mathcal{E}_1,\ Right$	0.0806	-
$\mathcal{E}_2,\ Left$	0.2420	-
$\mathcal{E}_2,\ Right$	0.0755	-

Table 13: Feature performance using the band-pass method and TF estimate, females. No significant disease-group difference was found.

Feature & Hemisphere	p	Significance
$\mathcal{E}_1,\ Left$	1.0000	-
$\mathcal{E}_1,\ Right$	0.5970	-
$\mathcal{E}_2,\ Left$	0.9699	-
$\mathcal{E}_2,\ Right$	0.5711	-

Table 14: Feature performance using the band-pass method and TF estimate, males.

4.2.3 Power in Frequency Bands

Here we shall, separately, consider the adapted approach of power in frequency bands. p-values for this analysis using band-pass method and the PSD are shown in Table 15. The frequency f_0 from 2.19 was chosen, empirically to be 365 Hz. This empirical selection was a simple case of 'band-finding' by visual inspection.

Feature & Hemisphere	p	Significance
$\mathcal{P}$ *Left, Females*	**0.0034**	***
$\mathcal{P}$ *Right, Females*	0.2545	-
$\mathcal{P}$ *Left, Males*	**0.0192**	*
$\mathcal{P}$ *Right, Males*	0.5970	-

Table 15: Using proportion of spectral energy $>$ 365 Hz as $\mathcal{P}$, p-values separating disease-groups were found in the left hemispheres of both genders.

As seen in Table 15, some significant results were found, and these are accounted for graphically in Figures 15 (females) and 16 (males) below.

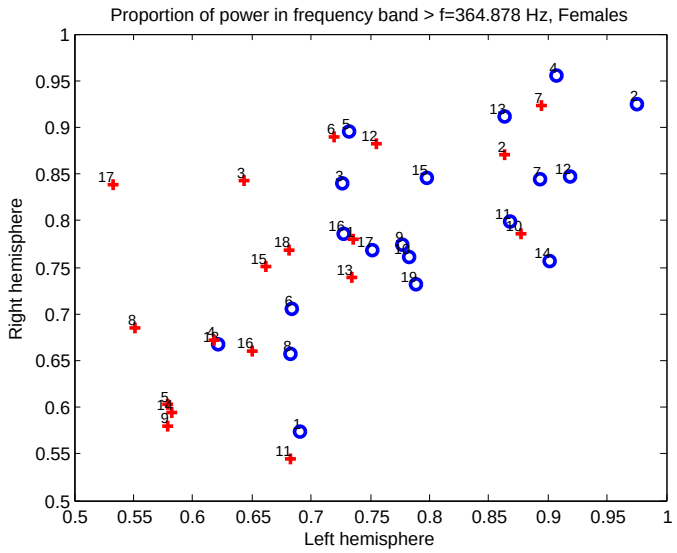

Figure 15: Feature space $\mathcal{P}$ for females. $p = 0.0034$ (***) in left hemisphere.

It is interesting to note, judging by Figures 15, 16, and to be discussed in Section 5.1, that whereas there appears to be less power in spectral bands for females diagnosed with ADHD, the reverse is true for males.

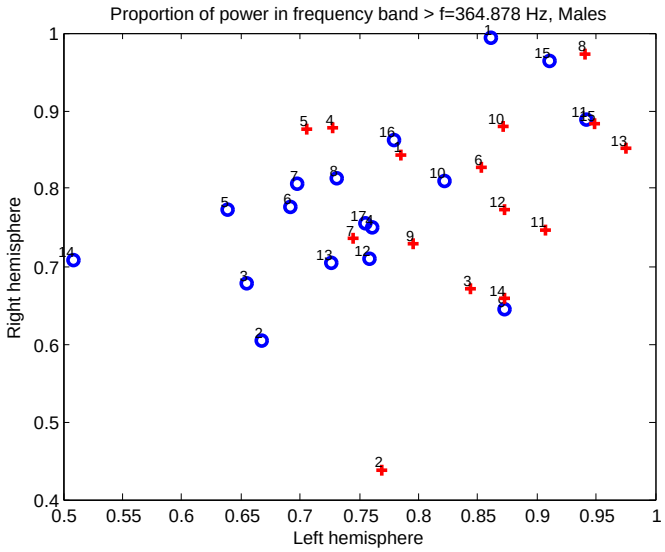

Figure 16: Feature space $\mathcal{P}$ for males. $p = 0.0192$ (*) in left hemisphere.

4.3 Feature Correlation

Having established features for each person, method and spectral representation, it may be of interest to compute somecorrelations between features. This is done for the female group and PSD estimate, and herein $\Theta_{b-p,PSD,\mathcal{H}_1,F,L}, \Theta_{b-p,PSD,\mathcal{H}_2,F,L}, \Theta_{b-p,PSD,\mathcal{I},F,L}$ on merit of these yielding significant results and on the same brain hemisphere. Consider the matrix $\boldsymbol{\rho}$ in Equation 4.1.

$$\boldsymbol{\rho} = \begin{matrix} 1 & -0.5261 & 0.8625 \\ -0.5261 & 1 & -0.8675 \\ 0.8625 & -0.8675 & 1 \end{matrix} \tag{4.1}$$

These are the correlations between, in order, $\mathcal{H}_1$, $\mathcal{H}_2$ and $\mathcal{I}$, both disease-groups have been used. Evidently, and as hinted at in Section 2.2, there is strong negative correlation between $\mathcal{H}_2$ and $\mathcal{I}$, -0.8675. Indeed, this needs to be taken into consideration when using both in a common classification space, such as below.

4.4 Classification in Feature Space

Having achieved the four instances of significance using PSD with the band-pass method in the female group (seen in Table 9) we may make an attempt at classification using these. Simple k-closest neighbour classification is adopted with $k = 1, 3, 5$ in the space

$$\{\Theta_{b-p,PSD,\mathcal{H}_1,F,L}, \Theta_{b-p,PSD,\mathcal{H}_2,F,L}, \Theta_{b-p,PSD,\mathcal{I},F,L}, \Theta_{b-p,PSD,\mathcal{K},F,R}\} \tag{4.2}$$

as these are the features giving rise to significant results in Table 9. The result of the classification attempt can be seen in Table 16 below.

	$k=1$	$k=3$	$k=5$
Sensitivity	72.22%	61.11%	66.67%
Specificity	63.16%	78.95%	78.95%

Table 16: Sensitivity (the number of females with ADHD correctlty classified) and Specificity (the number of females in the control group correctly classified) by means of k-closest neighbour algorithm with $k = 1, 3, 5$ in the space in Equation 4.2.

As an alternative, we may work under the assumption that results with relatively low significance may be coincidental due to the great number of tests. Then these, $\Theta_{b-p,PSD,\mathcal{H}_1,F,L}, \Theta_{b-p,PSD,\mathcal{K},F,R}$, ay be considered not viable as

traits to be used in a classification context and could be excluded from the space in Equation 4.2, rendering a new feature space for classification:

$$\{\Theta_{b-p,PSD,\mathcal{H}_2,F,L}, \Theta_{b-p,PSD,\mathcal{I},F,L}\}\,. \tag{4.3}$$

The same k-closest neighbour algorithm as above is applied, rendering results seen below in Table 17.

	$k=1$	$k=3$	$k=5$
Sensitivity	61.11%	61.11%	66.67%
Specificity	78.95%	47.37%	47.37%

Table 17: Sensitivity (the number of females with ADHD correctlty classified) and Specificity (the number of females in the control group correctly classified) by means of k-closest neighbour algorithm with $k = 1, 3, 5$ in the space in Equation 4.3. Evidently, downsizing the dimension of the classification space produces results that are, in the most part, not as good as keeping all significant features.

These classification attempts certainly do not perform an astonishing degree of accuracy, and can be viewed as a sketch for how classification *may* be conducted, given better traits than the ones here considered.

5 Conclusions

5.1 Discussion and Research Suggestions

From a clinical viewpoint, a primary problem using ADHD disease group data is the vagueness of the disease itself. As described in Section 1.2, there is much concern around mis- and over-diagnosis. Also, since the condition is far from life-theatning or indeed particularly critical, we can never be sure that any person partaking as a 'control' would *not* be diagnosed with ADHD if establishing contact with a psychiatrist. In all, this complication might imply that *even if* ADHD is a completely valid diagnosis and any quantitive method using existing features *is optimally proficient* at capturing some neural activity central to the disease, it will find similarities between control subjects with ADHD-like traits, as well as between the 'mis-diagnosed' and the non-carriers.

For all purposes, especially when computing the mean over observations, in 3.5 we made the assumption that v from Equation 3.3 is essentially equal between observations. This needn't be the case. In fact, it is not uncommon practise to model ERP-observations as a sum of signal and noise where *both* are realizations of stochastic processes. Here, amplitude, frequency and latency (i.e. phase) of the signal may all be stochastic. The case of amplitude is not relevant to this study, as all observations are normalized (c.f. Section 3). In the cases of variable frequency and latency, this will cause an averaging to act as a low pass filter [50], introducing potentially 'false' lower frequencies for subjects displaying great variations in these respects. Indeed, such an effect could indeed serve as a measure of frequency and/or latency shift but as this is not discernible from more constant low frequencies it is not a recommended marker for these effects. To mitigate the problem of variable latency between observations, a common technique is *aligned averaging* [50, p. 207], whereby observations are shifted in time based on optimization of correlation between them. When studying only spectra, such as in this study, this is certainly a viable approach to consider.

Indeed, another vital aspect overlooked with regards to the averaging is the distribution of the noise, which is not necessarily independent nor identically distributed between observations. Although this assumption is common and convenient it certainly needn't be the case, limiting the stringency and relevance of any mean valueing for noise-reduction. However, as noted in 3.1, the time between stimuli are varied in such a way that, from a viewpoint of measurement, a most vital action has been taken as to improve the independence between non-ABR activity between observations.

The window method was suggested by the author as a way to empirically

study the raw data material and try to filter the higher frequencies. It was later realized that lower frequency disturbances were prominent, and this method did not perform well. Perhaps, in order to remove spike artifacts, c.f. Figure 7, some form of median windowing is still of relevancy in *combination* with band-pass filtering.

Since $\mathcal{P}$ was not implemented until late in the working stages of this project, it has not been included as a dimension in 4.4, or in the correlation analysis of 4.3. Such an inclusion may well be interesting, and is indeed a suitable 'first continuation' if only taking off from this study alone. In which ever case, there was a certain gender discrepancy seen in $\mathcal{P}$, namely that females with ADHD tended to display lower energy in the high spectral band, while males with ADHD saw higher energy in this band. Maybe, people are being diagnosed with un-gender-like behaviour? This is certainly as far-fetched as any type of interpretation made here will be.

It was as noted in Section 2 that we are less interested in finding particularly well-resolved and leakage-free spectral components and more concerned with examining feature performance. Naturally, improving on the spectral and time-frequency estimates is, as always, advisable. Some suggested improvements are adopting more sophisticated stationary techniques, such as Welch's method [46]. In the case of TFD:s, an exciting continuation could be the reassignment method [48].

The 'ideal' ABR shown in 3 is the established way of regarding ABR:s. In terms of time-span, it can be concluded that this study has considered data up to 15 ms instead of 10, as can be seen in Figure 7 (c,d). This means that what is believed to be cognitive auditory processing responses show up within the time-span, which has evidently complicated matters. In using the band-pass method, time was limited to ~ 11.7 ms. For reasons mentioned; the foundation of '10 ms ABR' in clinical theory, and the subjects seen whose raw data mean observations resembled those of Figure 7, it is strongly suggested for any further study to consider only 10 ms post-stimuli.

There are good reasons to chose 1000 Hz as a good upper cutoff frequency in band-pass filtering ABR-data. This is due to the fact that, as mentioned in 1.3, 1 ms is a commonly accepted lower limit for action potential duration. The lower cutoff frequency used as described in 3.5 is however in no way obvious. Indeed, it has been suggested by personnel at SensoDetect (c.f. Section 3.1) that such a frequency ought to be lower. However, such a high frequency as 250 Hz was chosen as to reduce the later 'cognitive' responses as shown in Figure 7 c,d. If one considers less data than, as became the case with the band-pass filter method 11.7 ms (perhaps down to10 ms) one could consider lowering this cutoff frequency as not to lose potentially vital

information.

One interesting aspect of the results presented above is that, almost exclusively, significant differences between disease-groups were found in the left hemisphere. The well established findings regarding the lateralization of brain function[57][22], i.e. how some tasks are carried out by primarily one or the other, could perhaps serve as part of an explanation. Possibly, if the findings of more apparent group-differences in the left hemisphere is considered important, lateralization could come into play here. Two conceivable effects might then be that the left hemisphere is more 'accesible', in general, to examination for individual hearing characteristics or that there are specific abnormalities in the functions particular to the left hemisphere that correlate with ADHD as a disease.

Lastly, it is important to note that any of the low significance levels (*, $\alpha < 0.05$, and potentially (**), $\alpha < 0.01$) obtained should be put into great question. Based on the sheer number of statistical tests, we can expect false positives in our outcome. It can however be deemed quite possible to be confident with findings on higher levels than (**).

5.2 Summary

This study has sought to find traits for ADHD among features of Auditory Brainstem Response spectral representations. Data from any type of purpose-specific cerebral measurement, such as ERP/ABR, is always haunted by artifacts and noise in different frequency ranges, and this case has been no exception to that rule. With the need of data pre-processing, a window method proposed by the author was implemented. This was based on some curiosity around sliding windows in individual observations, and an empirical outlook on early visual inspection of data. However, it was quickly gathered that low-frequency noise was present in the data, either in the shape of cross-observational EEG- or circuit-noises, or by what was assumed to be larger auditory responses from higher cerebral structures appearing at the end of the observations in some test subjects. The sample space of test subjects was reduced as to only contain subjects with relatively low such disturbances in data, but even with this limitation no significant results were found by means of the window method. It can however be argued that limiting the sample sizes naturally diminishes the possibility of achieving significance, whether the groups cluster relatively well or not.

A later adopted band-pass approach performed better; both on an initial stage where produced mean observations (Figure 9) that looked as if the

[22]Indeed, there is also evidence that the brains of men and women differ in some aspects of lateralization, for instance concering language processing.

problems seen in Figure 8 (c,d,e,f) were mitigated, but also in the sense that some significant results were in fact obtained, Section 4.2. In the female group, we saw particularly high significance using measures of $\mathcal{H}_2$ and $\mathcal{I}$ from the power spectral density, both on the left brain hemisphere. Naturally, these two measures are heavily (negatively) correlated, Equation 4.1, and it should come as no surprise that they perform well simultaneously. Hence, it is also important to note this dependency when considering any form of classification.

To examine ABR-spectra in terms of the power in frequency bands, $\mathcal{P}$, was a method implemented at a later stage, and certainly holds some promise

In summary, the author sees no reason whatsoever for abandoning time-dependent techniques when evaluating ABR for purposes of ADHD diagnostics, or any other disease for that matter. There are, however, some findings to suggested that features in ABR-spectra could serve as an extension of some decision-space or -algorithm based, as of now, solely on, for instance, latency. This statement, that some spectral features may well contribute to further understanding of ABR as a diagnostic tool, may be stated primarily due to the low dependency between measures of latency shifts and spectral content.

References

[1] Goldberg, I. et. al.; *Neuronal correlates of "free will" are associated with regional specialization in the human intrinsic/default network.* Consciousness and Cognition, September 2008.

[2] Borg, J. et. al.; *The serotonin system and spiritual experience.* American Journal of Psychiatry, November 2003, 160(11):1965-1969.

[3] Kassam, K.S. et. al.; *Identifying Emotions on the Basis of Neural Activation.* PLoS ONE. Jun2013, Vol. 8 Issue 6, p1-12.

[4] Smiljanica, R. et. al.; *Acoustic and Semantic Enhancements for Children With Cochlear Implants.* Journal of Speech, Language & Hearing Research. Aug2013, Vol. 56 Issue 4, p1085-1096.

[5] de Almeida Ribeiro, P.R. et. al.; *Controlling Assistive Machines in Paralysis Using Brain Waves and Other Biosignals.* Advances in Human-Computer Interaction, 2013, Vol. 2013, p. 1-95.

[6] Micera, S. et. al.; *Hybrid bionic systems for the replacement of hand function.* Proceedings of the IEEE Sept. 2006, vol.94, no.9, pp. 1752-62.

[7] Neubert, F. et. al.; *Comparison of human ventral frontal cortex areas for cognitive control and language with areas in monkey frontal cortex.* Neuron 2014 Feb 5; Vol. 81 (3), pp. 700-13.

[8] Kindermans, P.J. et. al.; *A unified probabilistic approach to improve spelling in an event-related potential-based brain-computer interface.* IEEE Transactions on Biomedical Engineering Oct. 2013, vol.60, no.10, pp. 2696-705. ISSN: 0018-9294.

[9] Horowitz-Kraus, T. et. al.; *Overlapping neural circuitry for narrative comprehension and proficient reading in children and adolescents.* Neuropsychologia. Nov2013, Vol. 51 Issue 13, p2651-2662.

[10] Isoda, M. et. al.; *Cortico-basal ganglia mechanisms for overcoming innate, habitual and motivational behaviors.* European Journal of Neuroscience. Jun2011, Vol. 33 Issue 11, p2058-2069.

[11] Tusche, A. et. al.; *Automatic processing of political preferences in the human brain.* NeuroImage, Vol 72, May 15, 2013. pp. 174-182.

[12] Tuschman, A.; *Our Political Nature p 31-32* Prometheus Books.

[13] Sánchez-Lara, K. et. al.; *Brain activity correlated with food preferences: a functional study comparing advanced non-small cell lung cancer patients with and without anorexia.* NeuroImage, Vol 72, May 15, 2013. pp. 174-182.

[14] Chen, I.; *The court will now call its expert witness: the brain.* Stanford Report, November 19, 2009.

[15] Hamshere, M.L. et. al.; *High loading of polygenic risk for ADHD in children with comorbid aggression.* American Journal of Psychiatry, 2013 Aug 1; 170 (8): 909-16.

[16] Scharf, M. et. al.; *Adolescents' ADHD symptoms and adjustment: The role of attachment and rejection sensitivity.* American Journal of Orthopsychiatry, Vol 84(2), Mar, 2014. pp. 209-217.

[17] Centers for disease control and prevention; *ADHD Throughout the Years.* http://www.cdc.gov/ncbddd/adhd/documents/timeline.pdf.

[18] Beck, M.; *Mind Games: Attention-Deficit Disorder Isn't Just for Kids. Why Adults Are Now Being Diagnosed, Too.* Wall Street Journal Online (Health Journal).

[19] Rettew, D.; *The ADHD Debate.* Psychology Today Online, January 6, 2014 ABCs of Child Psychiatry.

[20] Huffington Post Portal; http://www.huffingtonpost.com/tag/adhd-debate/.

[21] Singh, I.; *Why are so many adults convinced that Ritalin does children harm?* The Daily Telegraph Online, 15 Oct 2012.

[22] Levy, F. et. al.; *Dopamine receptors and the pharmacogenetics of side-effects of stimulant treatment for attention-deficit/hyperactivity disorder.* Journal of Child and Adolescent Psychopharmacology, Vol 23(6), Aug, 2013. pp. 423-425.

[23] http://www.rxlist.com/ritalin-drug/patient-images-side-effects.htm

[24] Carnevale, N. T.; *The Neuron Book.* Cambridge University Press; 1 edition.

[25] McGlannan, F.; *Physiology – Brain Evolution.* Journal of Learning Disabilities; May1974, Vol. 7 Issue 5, p291-292.

[26] Okhrei, A.G. et. al.; *Specificity of Auditory Cognitive Evoked Potentials in Musicians.* Neurophysiology, Vol. 43, No. 6, March, 2012.

[27] Dornan, B. et. al.; *Pediatric hearing assessment by auditory brainstem response in the operating room.* International Journal of Pediatric Otorhinolaryngology. (International Journal of Pediatric Otorhinolaryngology, July 2011, 75(7):935-938).

[28] Källstrand, J. et. al.; *Lateral asymmetry and reduced forward masking effect in early brainstem auditory evoked responses in schizophrenia.* Psychiatry Research 30 April 2012 196(2-3):188-193.

[29] Cohen, C.I. et. al.; *Characteristics of Auditory Hallucinations and Associated Factors in Older Adults with Schizophrenia.* American Journal of Geriatric Psychiatry (AM J GERIATR PSYCHIATRY), 2014 May; 22 (5): 442-9.

[30] Källstrand, J. et. al.; *Abnormal auditory forward masking pattern in the brainstem response of individuals with Asperger syndrome.* Neuropsychiatric disease and treatment, 2010.

[31] Adams, J.C. et. al.; *Dorsal nucleus of the lateral lemniscus: a nucleus of GABAergic projection neurons.* Brain Res Bull 13(4): 585-90.

[32] Douglas, L.O. et. al.; *Axonal projections from the lateral and medial superior olive to the inferior colliculus of the cat: A study using electron microscopic autoradiography.* Journal of Comparative Neurology Volume 360, Issue 1, pages 17âĂŞ-32, 11 September 1995.

[33] Kolb, B.; Whishaw, I.Q.; *Introduction to Brain and Behavior* Worth Publishers, Third edition.

[34] Middlebrooks, J.C.; *Auditory System: Central Pathways.* Squire. Encyclopedia of Neuroscience. Academic Press. pp. 745 – 752.

[35] Barnett, M.W.; Larkman, P.M.; *The action potential: How to understand it.* Pract Neurol 2007;7:192-197.

[36] Li, R. et. al.; *Investigation of the critical geometric characteristics of living human skulls utilising medical image analysis techniques.* International Journal of Vehicle Safety 2 (4): 345 – 367.

[37] Verma, R. et. al.; *Sex differences in the structural connectome of the human brain.* Proceedings of the National Academy of Sciences of the United States of America. 1/14/2014, Vol. 111 Issue 2, p823-828.

[38] Goodrich, K.; *The Gender Gap: Brain-Processing Differences Between the Sexes Shape Attitudes About Online Advertising.* Journal of Advertising Research. Mar2014, Vol. 54 Issue 1, p 32-43.

[39] Salimi-Khorshidi, G. et. al.; *A meta-analysis of sex differences in human brain structure.* Neuroscience and Biobehavioral reviews; Feb, 2014, 39 p 34-p50.

[40] Bauermeister, J.J. et. al.; *ADHD and gender: are risks and sequela of ADHD the same for boys and girls?* Journal of Child Psychology & Psychiatry. Aug2007, Vol. 48 Issue 8, p 831-839.

[41] Nagaraj, H.C. et. al.; *Acquisition and analysis of brainstem auditory evoked responses of normal and diseased subjects by spectral estimation.* Frontiers of Medical & Biological Engineering. 2000, Vol. 10 Issue 1, p 67-75.

[42] Petoe, M.A. et. al.; *Spectral and synchrony differences in auditory brainstem responses evoked by chirps of varying durations.* Journal of the Acoustical Society of America. Oct2010, Vol. 128 Issue 4, p1896-1907.

[43] Depoortere, H. et. al.; *Evaluation of the stability of sleep using Hjorths Descriptors.* Physiology & Behavior; OCT, 1993, 54 4, p785-p793.

[44] Blanco-Velasco, M. et. al.; *Nonlinear Trend Estimation Of The Ventricular Repolarization Segment For T-Wave Alternans Detection.* IEEE Transactions on Biomedical Engineering Oct. 2010, vol.57, no.10, pt.1, pp. 2402-12.

[45] Dutoit, T.; Marques, F.; *Applied Signal Processing.* Springer-Verlag New York Inc 2008.

[46] Stoica, P.; Moses, R.; *Spectral analysis of Signals.* Prentice Hall, 1997.

[47] Dmitrienko A. et. al.; *Pharmaceutical Statistics Using SAS: A Practical Guide.*

[48] Sandsten, M.; *Lecture Notes: Time-Frequency Analysis of Non-Stationary Processes.* Lund University, Centrum Scientiarum Mathematicum.

[49] Boualem B.; *Time Frequency Signal Analysis and Processing.*

[50] Sörnmo, L.; Laguna, P.; *Bioelectrical Signal Processing in Cardiac and Neurological Applications.* Elsevier Academic Press 2005.

[51] Lazár, I. et. al.; *Verification if sequential patterns in production using Information Entropy.* Tehnicki Vjesnik / Technical Gazette. Jul/Aug2013, Vol. 20 Issue 4, p669-676.

[52] Galich, N.E. et. al.; *Wavelets of the immunofluorescence distributions; Shannon entropies, their central moments and fractal dimensions for medical diagnostics.* Materials Physics and Mechanics 2010, vol.9, no.3, pp. 228-35. ISSN: 1605-2730.

[53] Sharma, L.P. et. al.; *Influence of Shannon's entropy on landslide-causing parameters for vulnerability study and zonation-a case study in Sikkim, India.* Arabian Journal of Geosciences May 2012, vol.5, no.3, pp. 421-31. ISSN: 1866-7511.

[54] Florio, V. et. al.; *Differential impairment of interhemispheric transmission in bipolar disease.* Experimental Brain Research; Oct, 2013, 230 2, p 175-p185.

[55] Vidal, J.R. et. al.; *Category-specific visual responses: An intracranial study comparing gamma, beta, alpha, and ERP response selectivity.* Frontiers in Human Neuroscience, Vol 4, Nov 11, 2010. ArtID 195.

[56] Ferri, R.R. et. al.; *Relationship between Delta, Sigma, Beta, and Gamma EEG bands at REM sleep onset and REM sleep end.* Clinical Neurophysiology, Vol 112(11), Nov, 2001. pp. 2046-2052.

[57] Hugdahl, K.; Westerhausen, R.; *The Two Halves of the Brain: Information Processing in the Cerebral Hemispheres*, 2010.

[58] https://www.stat.auckland.ac.nz/ wild/ChanceEnc/Ch10.wilcoxon.pdf

[59] Image courtesy of SensoDetectAB.

[60] Image courtesy of Alila Medical Media, shutterstock.com.

[61] Image made by author.